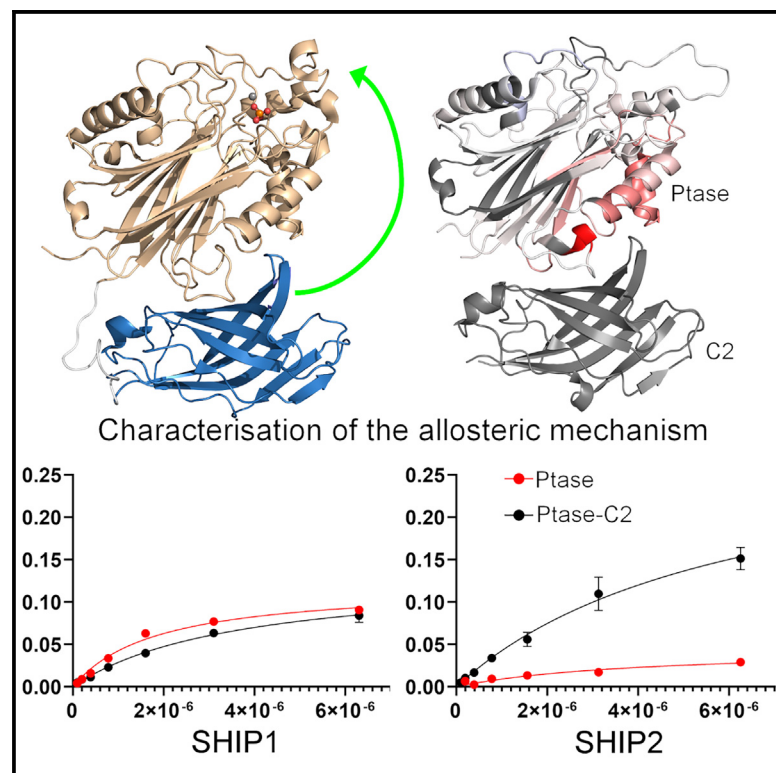


Structure

Regulation of inositol 5-phosphatase activity by the C2 domain of SHIP1 and SHIP2

Graphical abstract



Authors

William J. Bradshaw,
Emma C. Kennedy, Tiago Moreira, ...,
Paul E. Brennan, Emma J. Murphy,
Opher Gileadi

Correspondence

william.bradshaw@cmd.ox.ac.uk
(W.J.B.),
opher.gileadi@ki.se (O.G.)

In brief

Inositol 5-phosphatase SHIP1 is a potential target in Alzheimer's disease. Here, Bradshaw et al. present the structure of the phosphatase and C2 domains of SHIP1, explore the mechanism by which the C2 domain modulates phosphatase activity, and use two screens to identify novel SHIP1 binders.

Highlights

- Apo, and Mg^{2+} and PO_4^{3-} -bound structures of the phosphatase and C2 domains of SHIP1
- Characterization of allostery by the C2 domain using activity assays, HDX-MS, and MD
- Comparison to SHIP2 and other inositol 5-phosphatases
- A crystallographic fragment screen and MS screen to identify novel binders



Article

Regulation of inositol 5-phosphatase activity by the C2 domain of SHIP1 and SHIP2

William J. Bradshaw,^{1,5,*} Emma C. Kennedy,¹ Tiago Moreira,^{1,3} Luke A. Smith,² Rod Chalk,¹ Vittorio L. Katis,¹ Justin L.P. Benesch,² Paul E. Brennan,¹ Emma J. Murphy,¹ and Opher Gileadi^{1,4,*}

¹ARUK Oxford Drug Discovery Institute, Centre for Medicines Discovery, Nuffield Department of Medicine Research Building, Old Road Campus, University of Oxford, Oxford OX3 7FZ, UK

²Kavli Institute for Nanoscience Discovery, Dorothy Crowfoot Hodgkin Building, University of Oxford, South Parks Road, Oxford OX1 3QU, UK

³Present address: Astbury Center for Structural Molecular Biology and School of Molecular and Cellular Biology, Faculty of Biological Sciences, University of Leeds, Leeds, LS2 9JT, UK

⁴Present address: Structural Genomics Consortium, Center for Molecular Medicine, L8:02, Karolinska University Hospital, 171 77 Stockholm, Sweden

⁵Lead contact

*Correspondence: william.bradshaw@cmd.ox.ac.uk (W.J.B.), opher.gileadi@ki.se (O.G.)

<https://doi.org/10.1016/j.str.2024.01.005>

SUMMARY

SHIP1, an inositol 5-phosphatase, plays a central role in cellular signaling. As such, it has been implicated in many conditions. Exploiting SHIP1 as a drug target will require structural knowledge and the design of selective small molecules. We have determined apo, and magnesium and phosphate-bound structures of the phosphatase and C2 domains of SHIP1. The C2 domains of SHIP1 and the related SHIP2 modulate the activity of the phosphatase domain. To understand the mechanism, we performed activity assays, hydrogen-deuterium exchange mass spectrometry, and molecular dynamics on SHIP1 and SHIP2. Our findings demonstrate that the influence of the C2 domain is more pronounced for SHIP2 than SHIP1. We determined 91 structures of SHIP1 with fragments bound, with some near the interface between the two domains. We performed a mass spectrometry screen and determined four structures with covalent fragments. These structures could act as starting points for the development of potent, selective probes.

INTRODUCTION

SH2-containing inositol 5-phosphatases (SHIP1 and SHIP2) are key parts of the PI3K/AKT/mTOR signaling pathway. SHIPs dephosphorylate phosphatidylinositol-3,4,5-trisphosphate (PI(3,4,5)P₃) to produce phosphatidylinositol-3,4-bisphosphate (PI(3,4)P₂). The balance between these two second messengers and related phosphatidylinositol phosphates affects multiple cellular processes including inflammation, autophagy, cell migration, metabolism, and cell growth.^{1,2} Therefore, it is not surprising that SHIPs have been implicated in many conditions, including a range of cancers,^{3–5} diabetes,⁶ hypertension,⁷ and graft versus host disease.⁸

Genome-wide association studies have demonstrated a link between SNPs rs10933431 in intron 2 and rs35349669 in intron 10 of the *INPP5D* gene (SHIP1) and increased expression of SHIP1 in late-onset Alzheimer's disease (LOAD) in Caucasians.^{9,10} It has been shown, however, that the effects of these SNPs may not be straightforward. While the latter of the two mutations is linked with increased risk of LOAD in Caucasians, it does not appear to result in increased risk of LOAD in the Han Chinese population and the former appears to be protective.^{11,12}

The link between SHIP1 and Alzheimer's disease (AD) is believed to arise through its role in inflammatory processes in

the brain, specifically through the regulation of microglia and cytokine release via signaling from TREM2 and DAP12.^{13–17} Expression of the two SHIPs varies between tissues.^{18,19} In the brain, *INPP5D* expression is enriched in microglia, with much lower levels of transcripts detected in other cells. SHIP2 (*INPPL1*) has a lower level of expression but this is more consistent across different cells, including microglia and astrocytes.²⁰ Doubt has recently been cast on whether the link to AD through microglial function is unique to SHIP1, or involves both SHIPs.²¹ Further complicating matters, SHIPs have roles that extend beyond their phosphatase activity, as they possess ubiquitin and SH3 binding sites, and their phosphatase-dependent and -independent roles overlap.^{22,23}

Clearly, an improved understanding of how the two SHIPs carry out their functions and their roles in AD and other conditions is required. A number of inhibitors and activators have been developed in recent years, including a pan-SHIP inhibitor and a SHIP2 inhibitor with 20-fold selectivity.^{21,24,25} The utility of many of these compounds is somewhat limited and better chemical probes, particularly ones that have been structurally engineered for affinity and selectivity, would prove invaluable.

The SHIPs possess an N-terminal SH2 domain, which mediates interactions with phosphorylated membrane proteins such as c-kit, DAP12, and others.^{14,26,27} This is followed by a



Table 1. Crystallographic and refinement statistics – outer shell statistics are given in brackets

	Apo	Mg PO4 bound	Z2738285202	Z1742148362	Z1763271112	Z56948267
Crystallographic statistics						
Space group	P2 ₁ 2 ₁ 2 ₁	P2 ₁ 2 ₁ 2 ₁	P2 ₁ 2 ₁ 2 ₁	P2 ₁ 2 ₁ 2 ₁	P2 ₁ 2 ₁ 2 ₁	P2 ₁ 2 ₁ 2 ₁
Cell dimensions (Å, °)	62.9 80.1 90.3 90 90 90	62.5 79.1 89.3 90 90 90	62.7 79.4 89.6 90 90 90	62.5 79.2 89.4 90 90 90	62.5 79.0 89.3 90 90 90	62.7 79.6 89.6 90 90 90
Resolution (Å)	80.1–1.48 (1.51–1.48)	59.2–1.09 (1.14–1.09)	79.4–1.40 (1.42–1.40)	79.2–1.45 (1.47–1.45)	62.5–1.30 (1.32–1.30)	51.4–1.40 (1.42–1.40)
R _{merge}	0.187 (3.948)	0.152 (2.190)	0.170 (2.324)	0.194 (3.638)	0.096 (2.308)	0.134 (2.517)
R _{pim}	0.062 (1.639)	0.030 (0.480)	0.070 (1.010)	0.081 (1.495)	0.040 (0.998)	0.057 (1.095)
CC _{1/2}	0.997 (0.385)	0.998 (0.601)	0.998 (0.444)	0.998 (0.453)	1.000 (0.581)	0.998 (0.422)
Mean <I/σI>	11.4 (1.2)	11.7 (1.4)	8.5 (1.1)	8.0 (0.7)	11.6 (0.7)	9.6 (1.1)
Completeness (%)						
Spherical	100.0 (99.3)	87.6 (37.0)	100.0 (100.0)	100.0 (100.0)	100.0 (100.0)	100.0 (100.0)
Ellipsoidal	N/A	94.2 (59.6)	N/A	N/A	N/A	N/A
Total reflections	1,488,660 (49,808)	4,301,505 (163,879)	1,166,735 (54,505)	1,021,758 (51,037)	1,390,256 (65,597)	1,064,015 (52,281)
Total unique reflections	76,674 (3,736)	159,826 (7,907)	88,594 (4,478)	79,287 (3,864)	109,198 (5,345)	88,912 (4,359)
Multiplicity	19.4 (13.3)	26.9 (20.7)	13.2 (12.2)	12.9 (13.2)	12.7 (12.3)	12.0 (12.0)
Refinement statistics						
R _{work} /R _{free}	0.173/0.201	0.136/0.157	0.137/0.190	0.144/0.218	0.144/0.191	0.133/0.190
RMSDs						
Bond lengths (Å)	0.013	0.011	0.013	0.013	0.012	0.013
Bond angles (°)	1.791	1.702	1.785	1.753	1.718	1.770
Ramachandran statistics (%)						
Favored	97.3	97.8	97.6	95.0	96.3	94.4
Allowed	2.7	2.2	2.4	5.0	3.7	5.6
Outliers	0	0	0	0	0	0
Average B-factors						
Protein	21.0	14.3	19.9	21.3	21.5	22.0
Ligand	N/A	7.7	22.9	26.8	31.1	26.9
Water	28.4	25.4	31.1	32.2	33.5	32.3
Number of Atoms						
Protein	3742	4153	3871	3835	3936	3888
Ligand	N/A	6	16	13	13	9
Water	374	491	528	482	536	495
PDB Code	6IBD	6XY7	8PDG	8PDH	8PDI	8PDJ

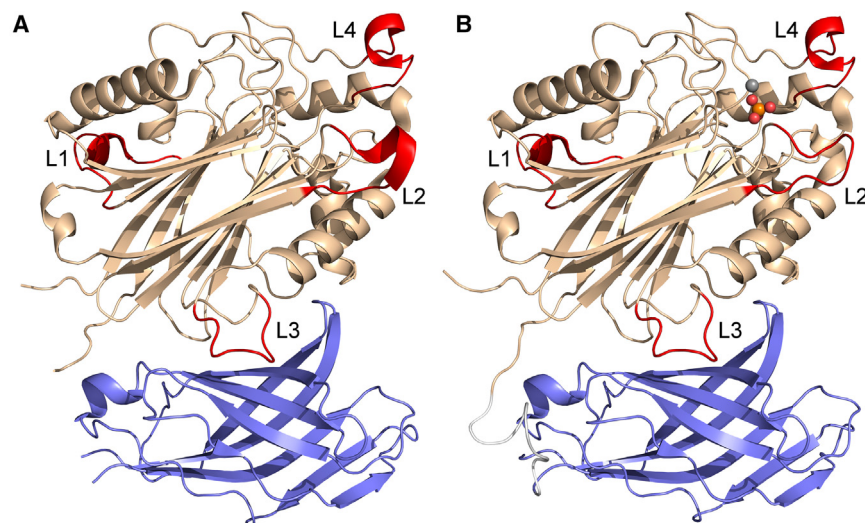


Figure 1. The structure of the phosphatase and C2 domains of SHIP1

(A) The apo structure. The phosphatase domain is colored brown and the C2 domain is blue. Loops 1 to 4 of the phosphatase domain, as numbered in Le Coq et al.³³ for SHIP2, are colored red. (B) The magnesium and phosphate bound structure, colored as in A. A magnesium ion (gray) and a phosphate ion (orange and red) are shown bound to the active site.

disordered region of approximately 60 residues and a dimerization/RhoA-binding domain.^{28,29} Centrally, they have a pleckstrin homology (PH) domain followed by a 5-phosphatase domain, a C2 domain, and a disordered region of approximately 300 residues. SHIP2 has a C-terminal ubiquitin interacting motif and a SAM domain.²³ The product of SHIP catalysis, PI(3,4)P₂, is believed to act as an allosteric activator of the inositol phosphatase activity, the C2 domain has been demonstrated to be essential to this: activators only work when the C2 domain is present.³⁰

The human genome codes for 10 inositol 5-phosphatases. Structures have been determined for 5: INPP5B, OCRL, SHIP2,³¹ synaptojanin-1,³² and INPP5E (PDB: 2XSW, Trésaugues et al., unpublished). While the active site is well conserved between these proteins, there are some differences that could be exploited if developing inhibitors. The structure of the phosphatase domain of SHIP2 with the C2 domain has also been determined.³³ The authors highlighted four loops (L1 to L4) in the phosphatase domain and suggested roles for three of them. L2 (K510 to G518 in SHIP1, K531 to G539 in SHIP2) was proposed to penetrate the membrane and deliver the substrate to the active site. L3 (D566 to N573 in SHIP1, D587 to D594 in SHIP2) interacts with the C2 domain and is thought to be important to transmitting the allosteric effects of the C2 domain to the active site in the phosphatase domain. L4 (T656 to N666 in SHIP1, N674 to N684 in SHIP2) forms the final part of this allosteric conveyor and part of the active site. Le Coq et al. proposed a mechanism of communication between the C2 and phosphatase domains through structures, activity assays on several mutants, and molecular dynamics.

Here, we present two high-resolution structures of the phosphatase and C2 domains of SHIP1: an apo structure and another with magnesium and phosphate bound to the active site. Comparison to other inositol 5-phosphatases reveals differences that are likely to be crucial for the development of selective compounds. We have explored the role of the C2 domain and the allosteric mechanism through activity assays, hydrogen-deuterium exchange mass spectrometry (HDX-MS), and molecular dynamics. These results provide evidence that the C2 domain is particularly important for SHIP2 activity, but

less so for SHIP1. We also present the results of a SHIP1 crystallography-based fragment screen, with 91 compounds bound that may serve as starting points for the development of inhibitors or degraders. We then performed a mass spectrometry (MS) screen of covalent binders and present a further 4 structures with covalent compounds bound.

RESULTS

The structure of SHIP1

We have determined the apo-structure of the phosphatase and C2 domains of human SHIP1 to a resolution of 1.48 Å, refined to R-factors of 0.173 and 0.201. We also determined a magnesium and phosphate-bound structure of the same domains with an elliptical high-resolution cutoff between 1.34 and 1.09 Å, refined to R-factors of 0.136 and 0.157 (Table 1). Each structure has one chain in the asymmetric unit and the structures superpose on each other with a root-mean-square deviation (RMSD) of 0.17 Å (Figure 1). Our structures are very similar to mouse SHIP1 (PDB: 6DLG), which was determined at approximately the same time (RMSDs of 0.29 Å (apo) and 0.27 Å (MgPO₄), identity of 95%).³⁴ They are also very similar to the phosphatase and C2 domains of human SHIP2 (PDB: 5OKM) with RMSDs between 0.59 and 0.80 Å, and an identity of 57% and the magnesium and phosphate-bound human SHIP2 structure (PDB: 5OKN), which has a D607A active site mutation.³³ The significantly higher resolution of the present magnesium and phosphate-bound structure compared to that of SHIP2 (1.34–1.09 Å vs. 2.65 Å) allows more precise positioning of the magnesium and phosphate ions, and orientation of the latter, within the active site and all waters bound to them, clarifying interactions within the active site (Figure 2). Most differences between the two structures can be ascribed to the difference in resolution. There are, however, some important differences between our magnesium and phosphate-bound structure, the magnesium and phosphate-bound OCRL structure (PDB: 4CMN),³¹ and the substrate-bound synaptojanin-1 structure (PDB: 7A17).³² Attempts were made to co-crystallize SHIP1 and to soak SHIP1 crystals with various inositol phosphates, but were unsuccessful. All structures presented here assume an L4-in conformation. This can be compared to structures of SHIP2 exhibiting either L4-in or L4-out conformations (Figure 2E), both of which are believed to be important to the catalytic mechanism and regulation of phosphatase activity by the C2 domain. While the

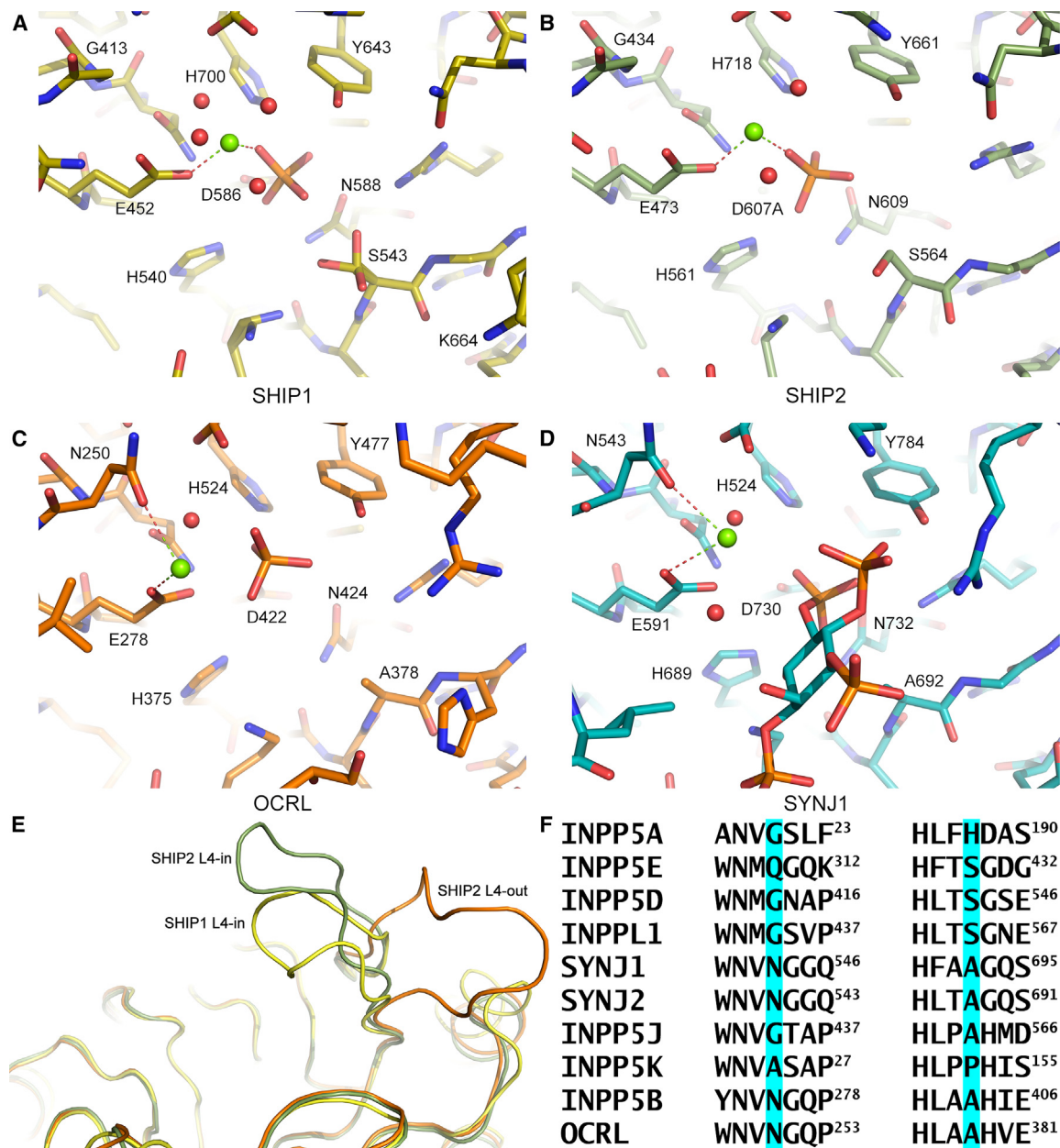


Figure 2. Active site comparison between INPP5 family members

(A) Magnesium and phosphate bound to the present SHIP1 structure (PDB: 6XY7). The magnesium is octahedrally coordinated by E542, the phosphate, and 4 waters. The phosphate is also bound to H540, S543, D586, N588, and H700.

(B) Magnesium and phosphate bound to SHIP2 D607A (PDB: 6OKN).³³ (C) Magnesium and phosphate bound to OCRL (PDB: 4CMN).³¹ As well as being coordinated by the phosphate and E278 (equivalent to E452 in SHIP1), the magnesium ion is also coordinated by N250, which is replaced by a glycine in the SHIPs. The phosphate is bound to E278, Y477, and H524 (equivalent to E542, Y643, and H700 in SHIP1).

(D) Magnesium and $\text{PI}(3,4,5)\text{P}_3\text{-DiC8}$ bound to synaptojanin 1 (PDB: 7A17).³² Magnesium binding resembles that of OCRL, while phosphate binding resembles that of the SHIPs, but with space for an attacking water.

(E) Comparison of L4 conformations above the active site between SHIP1 and SHIP2. The SHIP1 L4-in conformation from the magnesium and phosphate-bound structure is shown in yellow. The SHIP2 L4-in conformation is PDB: 3NR8 chain B, shown in green.³¹ The SHIP2 L4-out conformation is 5OKM chain B, shown in orange.³³

(F) Alignment of portions of the active site in each INPP5. Gly413 and Ser543 in SHIP1 and their equivalents in other INPP5s are highlighted in blue.

conformation of this loop does differ from that seen in the SHIP2 L4-in structure, PDB: 3NR8,³¹ care should be taken in overinterpreting differences due to potential packing artifacts in the present structures and in the SHIP2 structure.

Activity assays

To compare the catalytic activity of SHIP1 and SHIP2, and assess the effect of the C2 domain on phosphatase activity, we performed an activity assay to measure the phosphate

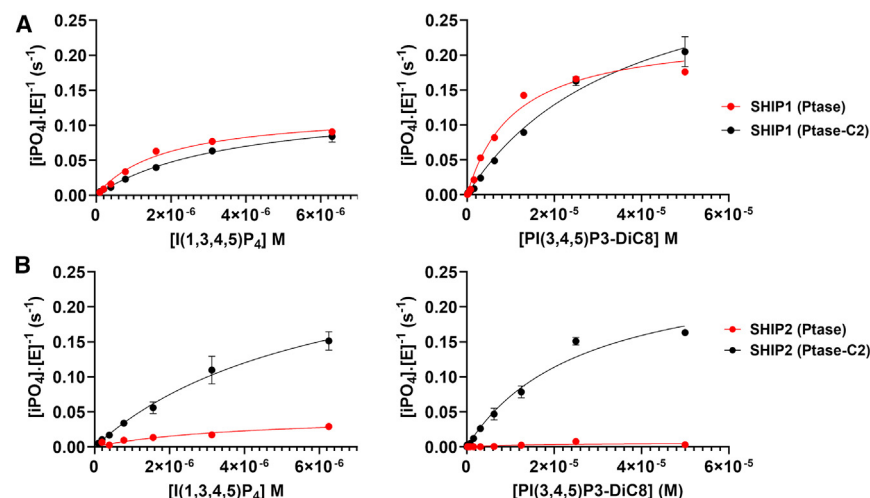


Figure 3. Activity assays

(A) Phosphatase activity of 50 nM SHIP1 against either I(1,3,4,5)P₄ (left) or PI(3,4,5)P₃-DiC8 (right). Initial rates have been plotted as phosphate produced per second per molar concentration of enzyme. There are no significant differences in the catalytic activity in the presence (black circles) or absence (red circles) of the C2 domain for either substrate.

(B) Phosphatase activity of 50 nM SHIP2 against either I(1,3,4,5)P₄ (left) or PI(3,4,5)P₃-DiC8 (right). As seen previously³³ the catalytic efficiency of SHIP2 is greater in the presence of the C2 domain (black circles) than the phosphatase alone (red circles). For I(1,3,4,5)P₄, the SHIP2 (Ptase-C2) was at 15 nM. n = 3. Data are represented as mean ± SEM.

produced by both the phosphatase domain alone (Ptase) and with the C2 domain (Ptase C2) on both SHIP1 and SHIP2 (Figure 3). The assay used a phosphate sensor, a fluorescently (MDCC) tagged *E. coli*-derived inorganic phosphate-binding protein with a lower limit of quantification in the picomolar range compared with the nanomolar range for malachite green, allowing accurate determination of phosphate produced at lower substrate concentrations. However, phosphate contamination of the substrates limited the usable range of concentrations, making K_m difficult to determine for low substrates. For each construct, K_m and k_{cat} were determined for PI(3,4,5)P₃-DiC8 and I(1,3,4,5)P₄ using the phosphate sensor assay (Table 2). These two substrates are water soluble alternatives that may not perfectly reflect the behavior of a membrane-bound substrate with longer acyl tails, but are commonly used analogs.^{31,32,35} For the Ptase-C2 constructs, the two proteins showed similar levels of activity for respective substrates, although for PI(3,4,5)P₃-DiC8, the k_{cat} of SHIP1 was approximately 50% higher than for SHIP2, while SHIP2 showed slightly higher activity for I(1,3,4,5)P₄ than SHIP1 did. For both substrates, SHIP2 showed a large increase in k_{cat} when the C2 domain was present, with more modest increases observed for substrate turnover of SHIP1. For both substrates, SHIP1 showed a slight increase in K_m in the presence of the C2 domain. SHIP2 showed a decrease in K_m , and therefore an increase in affinity for IP₄ with the C2 domain. The error in the calculated K_m of SHIP2-Ptase for PIP₃ was large due to very low activity, so no conclusion can be drawn about differences in K_m .

Hydrogen-deuterium exchange

To characterize the effect of the C2 domain on flexibility of the phosphatase domain, HDX-MS was performed on the constructs of SHIP1 and SHIP2 with and without the C2 domain (Figure 4). Deuterium uptake (DU) was measured for the SHIP1 constructs after 1, 10, and 30 min. For SHIP2, DU was measured at time points of 1, 2, 5, and 10 min. The HDX-MS data have been deposited with Oxford University Research Archive and can be accessed at <https://doi.org/10.5287/ora-py75jq8e5>. For SHIP1 after digestion with pepsin, 88 peptides were detected that were common between the two constructs, covering 88% of the phosphatase domain. For SHIP2, 70 shared peptides were

detected covering 86% of the phosphatase domain (Figure S1). While differences were observed in DU between Ptase and Ptase-C2, it is possible that for the most flexible regions, such as L4, shorter time points may have demonstrated a clearer difference. Almost all differences in DU that were observed showed greater DU in the shorter construct, with differences being more prominent for SHIP2 than for SHIP1. That is to say, Ptase constructs were more flexible/solvent accessible than the Ptase-C2 constructs. This is to be expected in regions normally buried in the interface between the two domains, but potentially not in more remote parts of the phosphatase domain. The greatest disparities were observed in residues approximately between 580 and 650 in SHIP2, encompassing part of $\alpha 4$ (helix 4), L3 (which interacts with the C2 domain), strand 9 (connecting L3 to the active site) and $\alpha 5$, $\alpha 6$, and $\alpha 7$. L3 and $\alpha 7$ in SHIP1 also showed the greatest degree of deprotection, but the effect on residues between these regions was less pronounced. Examples of regions where a statistically significant difference in DU was observed are shown in Figures S2 and S3.

Molecular dynamics

We conducted molecular dynamics to compare the relative flexibility of the SHIP1 and SHIP2 phosphatase domains in either the presence or absence of the C2 domain. Initially, we aimed to replicate the molecular dynamics simulations performed by Le Coq et al.³³ on SHIP2 starting from an L4-out conformation (Figures 5A and 5B) and complemented these with simulations on SHIP2 starting from an L4-in conformation (Figures 5C and 5D). We also performed simulations on SHIP1 L4-in (Figures 5E and 5F). Simulations could not be performed on SHIP1 L4-out as no such structure exists. These simulations were analyzed in two ways: firstly, we determined root-mean-square fluctuations (RMSFs) for C-alphas within the phosphatase domain, examining the effect of the C2 domain on the flexibility of the phosphatase domain, and particularly L4. Secondly, we calculated minimum distances across the simulations between K664/R682 (SHIP1/SHIP2) in L4 and neighboring acidic residues (D592 and E597 in SHIP1, D613 and D615 in SHIP2) that appear to stabilize the L4-out conformation, which were proposed by Le Coq et al.³³ to be residues that are involved in the signal network between the C2 domain and the active site.

Table 2. Activity Assays – errors are SEM

Phosphate Sensor	PI(3,4,5)P ₃ -DiC8		I(1,3,4,5)P ₄	
	K _m (μM)	k _{cat} (s ⁻¹)	K _m (μM)	k _{cat} (s ⁻¹)
SHIP1 Ptase	11.4 ± 1.6	0.24 ± 0.01	1.8 ± 0.2	0.12 ± 0.006
SHIP1 Ptase-C2	39.4 ± 5.7	0.38 ± 0.03	3.7 ± 0.4	0.13 ± 0.008
SHIP2 Ptase	19.3 ± 13 ^a	0.009 ± 0.003	6.90 ± 0.75	0.064 ± 0.003
SHIP2 Ptase-C2	26.6 ± 3.7	0.26 ± 0.02	2.7 ± 0.6	0.18 ± 0.02

^aVery low activity, poor fit to Michaelis-Menten.

Our simulations on SHIP2 L4-in showed the same general trends as those performed by Le Coq et al., i.e., L4 is more flexible and the hydrogen bonds stabilizing an L4-out conformation are more easily lost when the C2 domain is present; however, this effect was not as pronounced in our simulations. The simulations on SHIP2 L4-out indicated the opposite: that L4 is more flexible and the hydrogen bonds stabilizing an L4-out conformation are more easily lost when the C2 domain is *not* present. The simulations on SHIP1 L4-in showed mixed results; the C-alpha RMSFs suggested L4 is more flexible without the C2 domain while the minimum distances between K664 and D592 suggested that the presence of the C2 domain does not affect the ability of hydrogen bonds to form between these residues.

Crystallography-based fragment screen

To provide a starting point for the design of novel SHIP1 ligands, we performed a crystallography-based fragment screen on crystals of the phosphatase and C2 domains of SHIP1. Of the 597 fragments soaked into SHIP1 crystals, clear density was observed in PanDDA^{36,37} event maps for 91 compounds in 108 binding events (Figure 6) spread across 12 sites. Crystallographic and refinement statistics are given in data S1. 85 of these binding events occurred at one of two sites on either side of the phosphatase domain. As expected, no fragments were observed to be bound to the highly polar active site and the binding of many of the fragments was likely stabilized by crystallographic symmetry. There were, however, five fragments (PDB: 5RWD, PDB: 5RWL, PDB: 5RXV, PDB: 5RY9, and PDB: 5RYC) bound near to the interface between the phosphatase and C2 domains, including two fragments (5RXV and 5RYC) covalently bound to Cys505 (Figure 6C), which is not conserved in SHIP2. This finding presents a potential avenue for selectively targeting SHIP1 and modulating the interaction between the two domains and therefore possibly altering the activity of the phosphatase domain.

Mass spectrometry-based screen

As two fragments were observed to be covalently bound to SHIP1 in the crystallography-based screen, we conducted a mass spectrometry-based screen using an in-house library of 1920 covalent compounds (Figure 7A). Briefly, the protein was incubated overnight in the presence of each of the compounds and binding was assessed on an LC-ESI-TOF instrument. The results were inspected visually and the 20 strongest binders were selected for crystal soaks. Of these 20 compounds, 4 were observed to be covalently bound to Cysteine 505 in the resulting structures (Figures 7B; Table S1). For Z56948267 (PDB: 8PDJ), no density was observed for the nitrile group or the chloroacetyl group, which appear to have been lost.

DISCUSSION

The presented structures of SHIP1 allow comparison to SHIP2 and other inositol 5-phosphatases, highlighting differences that could be exploited for the development of selective modulators. The various structures of the SHIP2 phosphatase and C2 domains offer multiple “snapshots” of the structure.³³ The two proteins appear to differ more in the C2 domain than the phosphatase domain. Domains of the two proteins superpose with RMSDs between 0.38 and 0.41 Å for the phosphatase domain, and 0.67 and 0.82 Å for the C2 domain. In addition, relative orientations of the phosphatase and C2 domains differ slightly between SHIP1 and SHIP2. This difference appears to result from a hinging around the linker between the two domains. When the phosphatase domains are superposed, residues in the C2 domains near to the linker superpose well, but more distant residues do not. The C-alphas of Asp809 (SHIP1, MgPO₄-bound) and Asp829 (SHIP2, 5OKM chain G), for example, on the opposite side of the protein, are 3.2 Å apart. This hinging movement is supported by normal mode analysis with CCP4MG³⁸ indicating flexibility of the C2 domain. This flexibility is reflected in the C2 domain's higher B-factors compared to the phosphatase domain in both SHIP1 and SHIP2.

Substrate binding and catalysis

Inositol 5-phosphatases have been mechanistically compared to the distantly related apurinic/apyrimidic (AP) endonucleases.^{31,33} Competing hypotheses exist for the mechanism of AP endonucleases: either one³⁹ or two⁴⁰ metal ions are required for catalysis and, if the mechanism uses a single metal ion, this ion may move to different sub-pockets of the active site during the reaction (“site A” and “site B”). Recent developments on these hypotheses are summarized by Miroshnikova et al.⁴¹ It remains unclear, however, which is correct and to what extent this can be extrapolated to inositol 5-phosphatases. Regardless of the number of metal ions and their movement, the first step of the reaction is a nucleophilic attack on the 5-phosphate by a water deprotonated by Asp586/Asp607 (SHIP1/SHIP2). The magnesium and phosphate-bound structure of OCRL (PDB: 4CMN, Figure 2C) is believed to demonstrate the pre-catalytic positioning of the leaving phosphate with enough space between it and the catalytic Asp422 to accommodate the attacking water.³¹ This water, however, is not visible in the structure, likely due to the resolution of 3.13 Å. This resolution also limits the precision of the placement of the phosphate ion, the magnesium ion, and a coordinating water. Conversely, there is not enough space for the attacking water in our magnesium and phosphate-bound SHIP1 structure (Figure 2A), or the equivalent structure of SHIP2

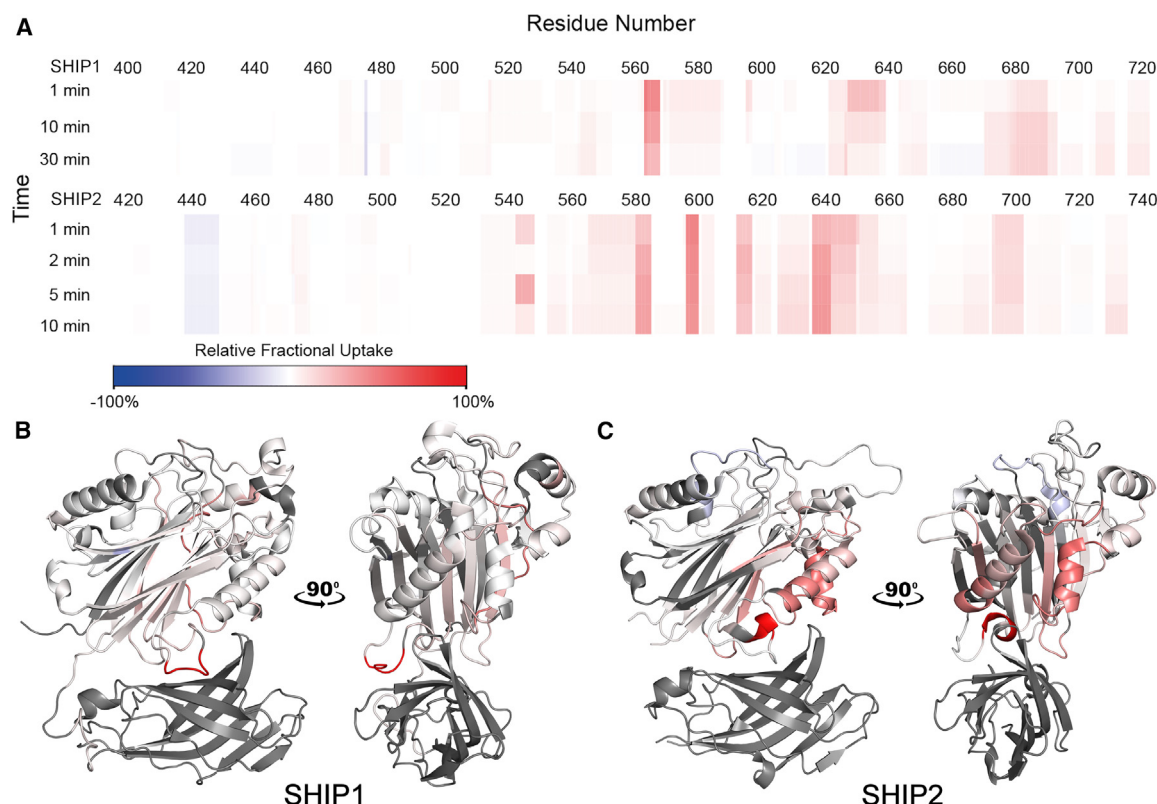


Figure 4. Hydrogen-deuterium exchange

(A) Differential heatmaps showing difference in deuterium uptake (Δ DU) between constructs with and without the C2 domain. Greater DU for the construct with the C2 domain is shown in blue while greater DU for the construct without the C2 domain is shown in red. Constructs without the C2 domain take up more deuterium and this effect is greater in SHIP2 than SHIP1.

(B) Δ DU for the 1 min time point mapped on to the structure of SHIP1 (6XY7). Regions not observed and the C2 domain are shown in gray.

(C) Δ DU for the 1 min time point mapped on to the structure of SHIP2 (5OKM chain B).

(PDB: 5OKN, Figure 2B). There is a direct interaction between Asp586/Asp607 and the phosphate, which in SHIP1 is approximately 2.3 Å away from its position in the OCRL structure. It was suggested that this represents the post-cleavage position of the 5-phosphate,³³ which our higher resolution SHIP1 structure seems to confirm.

The structure of the 5-phosphatase domain of synaptojanin-1 was recently determined with PI(3,4,5)P₃-diC8 bound to the active site.³² This is the first substrate-bound inositol 5-phosphatase structure. Despite a relatively low resolution of 2.73 Å, most of the substrate and active site residues have good density. The density for the magnesium ion and coordinating waters is somewhat lacking, slightly limiting the conclusions that can be drawn and the Check My Metal Server⁴² returns poor validation metrics for the magnesium ion. The orientation of the inositol ring and its distance from the magnesium ion suggests the possibility of a hydrated cation- π interaction.⁴³ The leaving phosphate is closer to the position seen in the present SHIP1 structure than in the OCRL structure, i.e., post-cleavage rather than pre-cleavage, despite the structure being substrate bound, the potential attacking water is also oddly positioned. The magnesium ion, on the other hand, is closer to the position seen in the OCRL structure than in the SHIP1 structure. Further high-resolution and substrate-bound structures will be

required to fully explain these differences and characterize substrate binding and the catalytic mechanism.

There are three notable differences between inositol 5-phosphatase active sites (Figure 2). Firstly, Gly413/Gly434 in SHIP1/SHIP2 is usually an asparagine in other INPP5s but may also be a glutamine or alanine. Secondly, Ser543/Ser564 is usually an alanine but may also be a histidine or proline. Additionally, L4 in the SHIPs is replaced with the shorter P4-interacting motif (P4IM) in other INPP5s. The first two of these differences are particularly notable since, in the OCRL and synaptojanin-1 structures, the asparagine coordinates the magnesium ion. As this coordination donor is not present in the SHIPs, since they contain a glycine at this position, any “pull” on the magnesium toward that specific part of the active site is lost, arguably resulting in the different binding of magnesium and phosphate seen in the SHIP structures. Instead, the phosphate is now weakly bound to the serine. The inference of weak binding is taken from the fact that this serine has clear density for 3 different conformations in our high-resolution structure, two of which place the oxygen 2.5 and 2.7 Å away from one of the phosphate oxygens. If it is argued that the positioning of the magnesium ion in the SHIP structures represents the post-catalytic position and the position in the OCRL and synaptojanin-1 structures represents the pre-catalytic position, how would the magnesium get into the

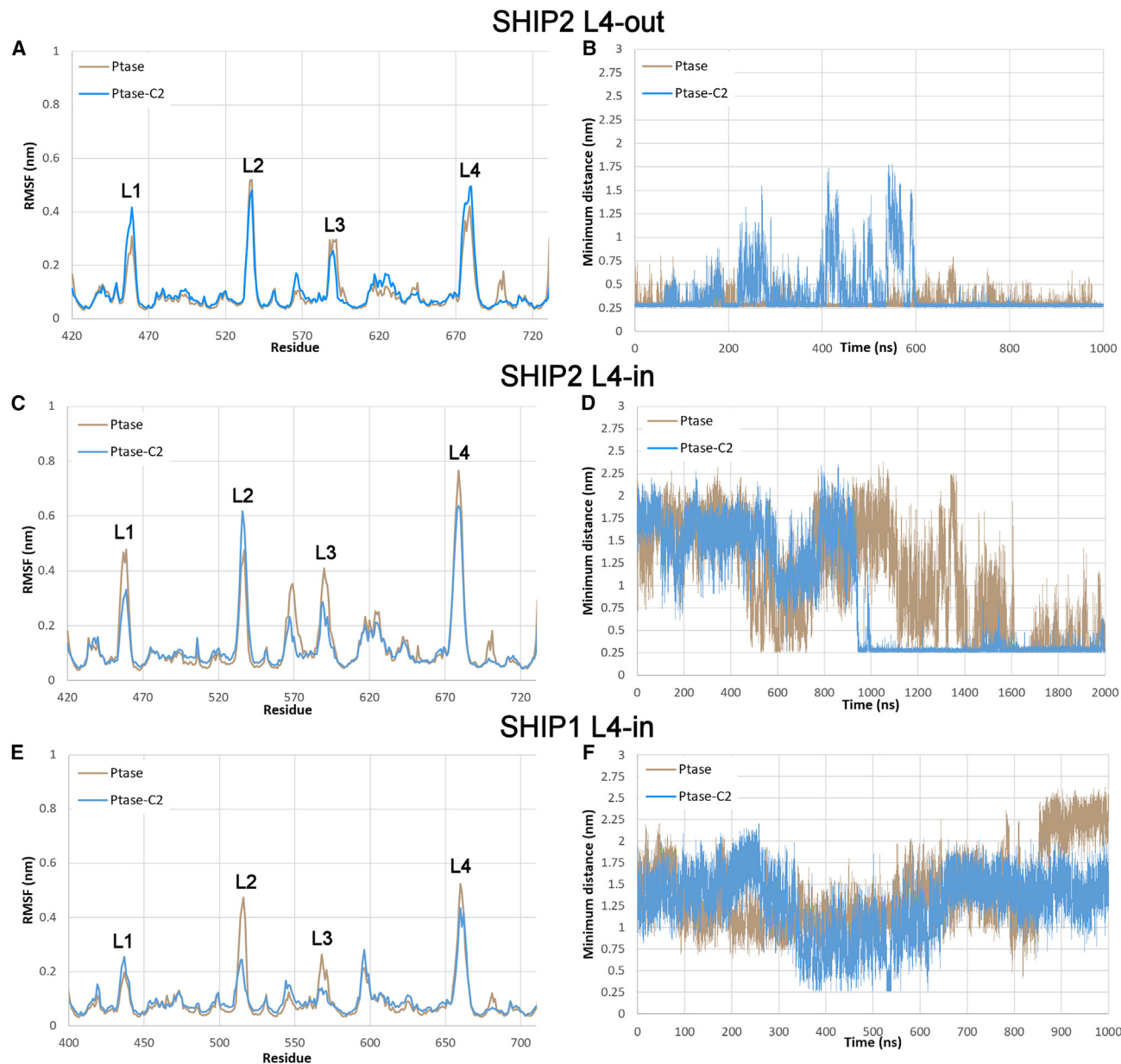


Figure 5. Molecular dynamics simulations

(A) SHIP2 L4-out. Our average ($n = 3$) RMSFs (root-mean-square fluctuations) from reproductions of the simulations performed by Le Coq et al.³³ This figure is equivalent to Figure 5A in Le Coq et al.³³ L1 to L4 are labeled.

(B) SHIP2 L4-out. Minimum distance between R682 and D613/D615 from reproductions of the simulations performed by Le Coq et al.³³ This figure is equivalent to Figure 5D in Le Coq et al.³³ and is a representative graph for 3 repeats.

(C) SHIP2 L4-in. Average RMSFs from simulations using 3NR8³¹ and 3NR8 with the C2 domain from 5OKM chain B.

(D) SHIP2 L4-in. Representative minimum distance between R682 and D613/D615 from simulations using 3NR8 and 3NR8 with the C2 domain from 5OKM chain B.

(E) SHIP1 L4-in. Average RMSFs from simulations using the present apo structure, 6IBD.

(F) SHIP1 L4-in. Representative minimum distance between K664 and D592/E597.

precatalytic position in the SHIPs, as it must do for catalysis to proceed? Does the substrate force the magnesium into the pre-catalytic position? Trésaugues et al.³¹ observed that SHIP2 is between 25 and 80 times less catalytically active than other inositol 5-phosphatases. It was suggested that this may simply be because the assay was not optimized for SHIP2. While their

assay only used the phosphatase domain of SHIP2, which both we and Le Coq et al.³³ have shown is considerably less active without the C2 domain, we have observed similarly lower levels of activity for both SHIP1 and SHIP2, comparable to that seen by Trésaugues et al.³¹ Thus, we propose that the differences in the active site favoring the binding of magnesium, and

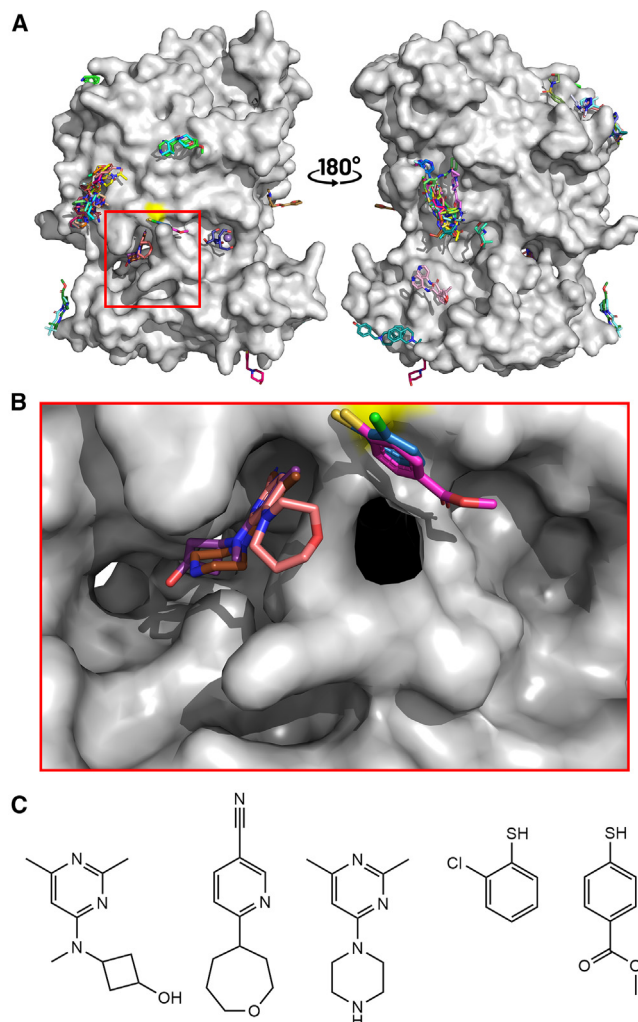


Figure 6. Crystallographic fragment binding

(A) A surface representation of the structure of SHIP1 is shown with the same orientation as Figure 1 and rotated 180°. The fragments from the 108 binding events are also shown.

(B) Fragments near to the interface between the phosphatase and C2 domain, including two covalently bound to C505 (yellow). Lys567 has been omitted for clarity.

(C) The five fragments bound near C505, with the two covalent fragments positioned on the right.

therefore phosphate, in the “product position” in the SHIPs, as opposed to OCRL which favors the “substrate position,” may be the reason for their lower activity. There also could be a degree of coevolution in these two residues (Figure 2F), suggesting that their roles in the mechanism are linked.

The third of the differences—the 11-residue L4 in SHIPs versus the 7 residue P4IM in other inositol 5-phosphatases—may play an important role in substrate specificity. The P4IM is so named because it closely interacts with the phosphate bound to position 4 of the inositol ring.³¹ The longer L4 still interacts with the 4-phosphate but is believed to fold over the top of the substrate, allowing K664/R682 (SHIP1/SHIP2) to interact with the phosphate in position 3.³³ While the SHIPs can cleave substrates without a 3-phosphate, they seem to be considerably more

active when the 3-phosphate is present. The role of L4 in conveying the allosteric effect from the C2 domain may explain this selectivity.

It has recently been shown that while the primary biological substrate of SHIP1 is PI(3,4,5)P₃, the protein is able to hydrolyze many substrates.⁴⁴ Likewise, SHIP2 has been shown to be capable of hydrolyzing several (phosphatidyl) inositol phosphates,⁴⁵ but notably, SHIP1 can hydrolyze I(2,3,4,5)P₄, whereas SHIP2 cannot. Nelson et al.⁴⁴ were unable to explain this observation. The active site is well conserved between the two SHIPs, except for part of L4 and N414/S435. The side chain of N414 seems to be well positioned to act as a hydrogen bond donor to a phosphate in position 2. It seems unlikely that any residues in L4 will be responsible for this substrate selectivity, so N414/S435 is the primary candidate. Regardless of the structural basis for this selectivity, this distinction may be the sole difference between the specificities of SHIP1 and SHIP2, which could potentially be exploited in the development of selective inhibitors that bind to the active site.

The allosteric mechanism

The allosteric effect of the C2 domain on phosphatase activity was explored in SHIP2 by Le Coq et al.³³ using a malachite green assay. It was observed that for I(1,3,4,5)P₄, the k_{cat} of Ptase-C2 was approximately 50% higher than for Ptase, while the K_m was marginally higher for Ptase-C2. They also observed that for PI(3,4,5)P₃-DiC8, the presence of the C2 domain resulted in an 11-fold increase in k_{cat} and a doubling of K_m . We carried out kinetic characterization for the SHIP1 phosphatase domain in the presence and absence of the C2 domain for I(1,3,4,5)P₄ and PI(3,4,5)P₃-DiC8 (Figure 3A). The same characterization was performed for SHIP2 (Figure 3B). In concordance with data shown by Le Coq et al.,³³ the C2 domain significantly enhances the catalytic activity of the phosphatase domain of SHIP2 and this effect is more pronounced for PIP₃ than for IP₄. In contrast, the C2 domain of SHIP1 appears to cause a moderate increase in catalytic activity for PIP₃ but has no significant effect on activity for IP₄, as has previously been observed.³⁰ Due to these differences, care should be taken in overinterpretation of data relating to IP₄ cleavage when PIP₃ is the physiological substrate.

Le Coq et al.³³ further characterized the allosteric effect in SHIP2 through activity assays on a series of mutants and molecular dynamics. It was concluded that the allosteric effect of the C2 domain is transmitted through Phe855 and Glu862 in the C2 domain, which interact with Arg649 just after $\alpha 7$. The allosteric effect then travels up the side of the phosphatase domain via $\alpha 7$ - $\alpha 5$ to a hydrogen bond network involving Asp613, Asp615 just before $\alpha 5$, and Arg682 in L4 (Figure 8). L4 forms part of the active site, allowing the C2 domain to modulate the flexibility of L4 between “L4-in” and “L4-out” conformations, thereby affecting substrate binding and product release. These charge-based interactions were determined to mainly affect interactions with the polar inositol head group, while less characterized hydrophobic interactions were said to affect binding to the acyl tails.

It seems logical that the allosteric mechanism would be conserved between SHIP1 and SHIP2. However, the first three residues identified in the allosteric mechanism, Phe855, Glu862, and Arg649, are not conserved (Figure 8). Of the latter three residues, Asp613/Asp592 (SHIP2/1) is conserved, while Arg682 (SHIP2) is exchanged for Lys664 (SHIP1). This may

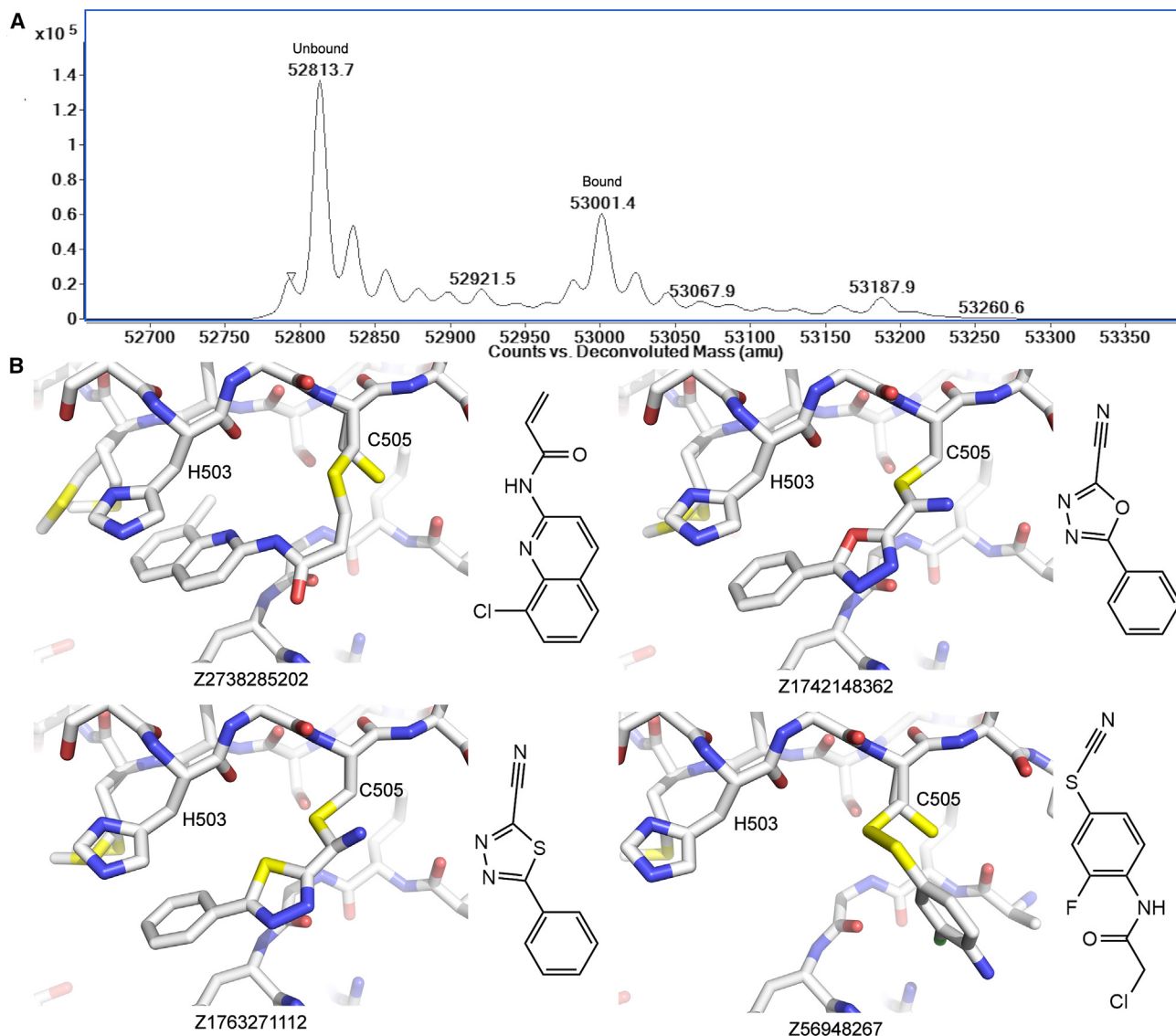


Figure 7. Mass spectrometry screen

(A) An example spectrum from the screen is shown. The unbound protein has a mass of 52813 and shows sodium adducts. The protein with a covalent ligand bound has a mass of 53001.

(B) The four compounds that were successfully soaked into SHIP1 crystals covalently bound to C505. To the right of each image, the structure of the unbound compound is shown. In the case of Z56948267, both the nitrile group and the chloroacetyl group were lost.

seem mechanistically acceptable, but lysine cannot form the number of hydrogen bonds hypothesized as important. Asp615 (SHIP2) is not conserved (Pro594 in SHIP1), but it is possible that its role is fulfilled by the nearby Glu597 (SHIP1). As our structures are in an L4-in conformation, they do not show hydrogen bonds between Lys664 and either Asp592 or Glu597. To shed further light on the allosteric mechanism and possible differences between SHIP1 and SHIP2, we replicated the molecular dynamics performed by Le Coq et al. on SHIP2 L4-out and performed the same simulations on SHIP2 L4-in and on SHIP1 L4-in. We also performed HDX-MS to investigate changes in the flexibility of the phosphatase domain caused by the absence of the C2 domain.

Our replication of the molecular dynamics (MD) performed by Le Coq et al. showed the same general trend, i.e., L4 is more flexible and the hydrogen bonds stabilizing an L4-out conformation are more easily lost when the C2 domain is present. This effect was not as pronounced in our simulations, however. SHIP2 L4-in simulations indicated the opposite: that L4 is more flexible and the hydrogen bonds stabilizing an L4-out conformation are more easily lost when the C2 domain is *not* present. While SHIP1 L4-in simulations indicated that the flexibility of L4 is largely unaffected by the presence of the C2 domain.

In the SHIP1 molecular dynamics simulations, regardless of the presence of the C2 domain or a hydrogen bond, Lys664 was always closer to Asp592, than Glu597, which is not the

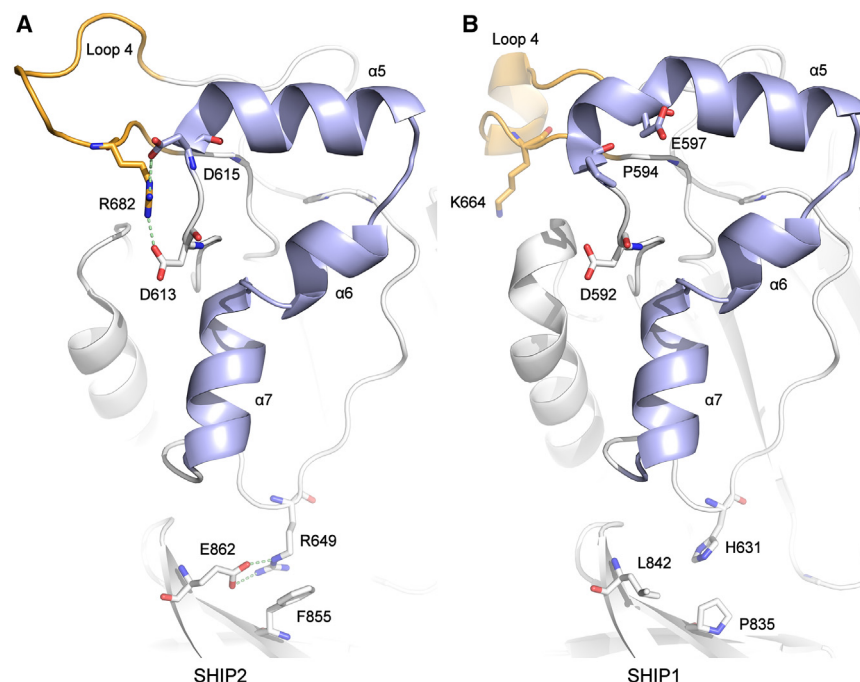


Figure 8. The proposed allosteric mechanism

(A) SHIP2 L4-out. Le Coq et al.³³ proposed that the effect of the C2 domain is conveyed from Phe855 and Glu862 to Arg649, up $\alpha 7$ - $\alpha 5$ (light blue), through Asp613 and Asp615 to Arg682 in L4 (orange), which is central to substrate binding. (B) SHIP1 L4-in. These residues are largely unconserved in SHIP1, leading to the absence of the required interactions.

case for the respective SHIP2 residues, suggesting that Glu597 in SHIP1 does not fulfill a role equivalent to that of Asp615 in SHIP2 and that the exchange of Arg682 for Lys664 and Asp615 for Pro594 results in a partial loss of the hydrogen bond network seen around L4 when SHIP1 is compared to SHIP2.

Our HDX-MS provides further insight into the allosteric mechanism proposed by Le Coq et al., who said that the C2 domain is able to modulate the flexibility of L4 via $\alpha 7$ - $\alpha 5$. The HDX-MS clearly demonstrated that in SHIP2, when the C2 domain is not present, L3, strand 9, and $\alpha 5$ - $\alpha 7$ had increased deuterium uptake, indicating increased solvent accessibility and/or flexibility. This effect was also seen in SHIP1 but to a lesser extent. L4 showed maximal deuterium uptake at the first time point for both SHIPs. This seems to indicate that the effect of the C2 domain is conveyed to the opposite side of the phosphatase domain by $\alpha 7$ - $\alpha 5$ but also by strand 9. Residues identified by Le Coq et al. may be involved in this mechanism and their lack of conservation may explain why the effect appears to be weaker in SHIP1. It seems that the C2 domain causes a significant degree of stabilization and decreased flexibility for one side of the phosphatase domain. Our molecular dynamics simulations do seem to reflect this to some extent. It does seem that, for L4-in simulations, at least, the phosphatase domain is marginally more flexible when the C2 domain is not present (Figures 5C–5E). Although this was not seen for the SHIP2 L4-out simulations (Figure 5A). The lack of effect either way seen in SHIP1 may reflect the decreased effect of the C2 domain.

The results from MD, combined with the results from HDX-MS and the lack of conservation of important residues between SHIP1 and SHIP2 seem to indicate that the allosteric mechanism hypothesized by Le Coq et al. is likely to hold some validity. Specifically, there appears to be some altered flexibility of $\alpha 7$ - $\alpha 5$, possibly influenced by the ability of the C2 domain to modulate the flexibility of one side of the phosphatase domain, potentially

through a hinging motion around the linker connecting the two domains. This modulation may impact the flexibility of L4 although our HDX-MS experiments did not reveal significant changes, possibly due to the lack of an early enough time point, and the observed changes in MD simulations were minimal. Notably, much of the hydrogen bond network around L4 in SHIP2 that was proposed to be involved in the mechanism is not conserved in SHIP1. The apparent

weaker effect of the C2 domain on the phosphatase domain of SHIP1 may mean that modulation of phosphatase activity by targeting the C2 domain is perhaps a more viable strategy for SHIP2 than for SHIP1. However, it is important to not entirely disregard the potential of targeting the C2 domain of SHIP1 as it does seem to still have some effect. Notably, it has been demonstrated that while removal of the C2 domain does not affect activity, addition of the product or an activator in the presence of the C2 domain can have a significant effect on activity.³⁰ It may therefore still be possible to target SHIP1 with an allosteric inhibitor.

Further to the work presented here, it has been demonstrated recently that the PH domain that precedes the phosphatase domain in both SHIP1 and SHIP2 is also able to modulate the activity of the phosphatase domain, in SHIP2, at least.³⁵ It has also been shown that the compound ZPR-MN100 is able to activate SHIP1, probably through binding to a pocket at the interface between the phosphatase and C2 domains, likely modulating the interaction between the two domains with Lys681 (mouse residue numbering, Lys677 in human) being essential to binding.³⁴ Thirdly, it has recently been shown that the SH2 domain of SHIP1 is able to autoinhibit phosphatase activity.⁴⁶ Further investigation into the mechanisms involved in all of these forms of modulation would potentially unlock opportunities to target other SHIP domains as strategies for developing small-molecule modulators.

Fragment-bound structures

We have presented 95 structures of SHIP1 with small molecules bound with 91 derived from crystallography-based fragment screening and 4 from a mass spectrometry screen. One of two sites at which the majority of binding events occurred in the crystallographic screen is in close proximity to the Lys677 pocket, to which it has been suggested ZPR-MN100 binds.³⁴ These compounds may provide potential ways in which this compound could be elaborated. We also observed five molecules from

the crystallographic screen bound to a pocket near to the interface between the phosphatase and C2 domains, of which 2 were covalently bound to Cys505, a residue not conserved in SHIP2. The 4 structures that contain compounds identified in the MS screen show the molecules covalently bound to the same cysteine residue. It is assumed that other hits from the MS screen that we were unable to determine structures for also bound to this cysteine. Many of the compounds identified in this study have been assayed for their ability to modulate SHIP1 activity (data not shown) but so far, all show minimal effects and should only be taken as starting points. Given their proximity to the interface between the two domains, compounds bound at this site have may modulate the activity of the phosphatase domain. Helix 4, which showed increased flexibility in the constructs without the C2 domain in HDX-MS analysis, is near this cysteine, providing a mechanism through which compounds bound to Cys505 may modulate phosphatase domain flexibility and therefore, activity.

We have presented here high-resolution structures of the phosphatase and C2 domains of SHIP1, assessed the role of the C2 domain in SHIP1 and SHIP2 using activity assays, HDX-MS, and molecular dynamics. While the C2 domain of both proteins can modulate the activity of the phosphatase domain through a seemingly conserved mechanism, the effect is considerably more pronounced in SHIP2 than in SHIP1, which we put down to the lack of conservation of specific residues identified as important to allosteric communication. We have also presented a crystallographic fragment screen on SHIP1 and followed this up with a mass spectrometry screen of covalent compounds, from which we were also able to determine a further four structures with covalent compounds bound. These structures will serve as starting points for the development of selective compounds able to modulate the activity of SHIP1 by targeting the allosteric mechanism discussed herein.

STAR★METHODS

Detailed methods are provided in the online version of this paper and include the following:

- **KEY RESOURCES TABLE**
- **RESOURCE AVAILABILITY**
 - Lead contact
 - Materials availability
 - Data and code availability
- **EXPERIMENTAL MODEL AND STUDY PARTICIPANT DETAILS**
- **METHOD DETAILS**
 - Cloning
 - Protein expression
 - Protein purification
 - Structure determination
 - Activity assays
 - Hydrogen-deuterium exchange
 - Molecular dynamics
 - Crystallography-based fragment screening
 - Mass spectrometry-based screen
- **QUANTIFICATION AND STATISTICAL ANALYSIS**

SUPPLEMENTAL INFORMATION

Supplemental information can be found online at <https://doi.org/10.1016/j.str.2024.01.005>.

ACKNOWLEDGMENTS

The authors would like to thank Diamond Light Source for beamtime (proposals lb22717, mx15433, and mx19301), and the staff of beamlines I03, I04, I04-1, and I24 for assistance with crystal testing and data collection. We thank the Alzheimer's Research UK Oxford Drug Discovery Institute (AR-UK2018DDI-0X) and the National Institutes of Health/National Institute on Aging (NIH/NIA) (1U54AG065187-01) for funding. We also thank William Kerr and Sandra Fernandes for the donation of the SHIP1-Ptase construct.

AUTHOR CONTRIBUTIONS

Conceptualization: W.J.B. and O.G.; data curation: W.J.B., E.C.K., R.C., and J.L.P.B.; formal analysis: W.J.B., E.C.K., T.M., L.A.S., E.J.M., and O.G.; funding acquisition: P.E.B. and O.G.; investigation: W.J.B., E.C.K., T.M., L.A.S., and O.G.; methodology: W.J.B., E.C.K., E.J.M., and O.G.; project administration: W.J.B. and O.G.; resources: R.C., V.L.K., J.L.P.B., P.E.B., and O.G.; supervision: W.J.B., R.C., V.L.K., J.L.P.B., P.E.B., E.J.M., and O.G.; validation: W.J.B., E.C.K., T.M., L.A.S., E.J.M., and O.G.; visualization: W.J.B., L.A.S., and E.J.M.; writing - original draft: W.J.B.; writing - review & editing: all authors.

DECLARATION OF INTERESTS

The authors declare no competing interests.

Received: August 1, 2023

Revised: December 12, 2023

Accepted: January 8, 2024

Published: February 2, 2024

REFERENCES

1. Eramo, M.J., and Mitchell, C.A. (2016). Regulation of PtdIns(3,4,5)P3/Akt signalling by inositol polyphosphate 5-phosphatases. *Biochem. Soc. Trans.* **44**, 240–252.
2. Viernes, D.R., Choi, L.B., Kerr, W.G., and Chisholm, J.D. (2014). Discovery and development of small molecule SHIP phosphatase modulators. *Med. Res. Rev.* **34**, 795–824.
3. Brauer, H., Strauss, J., Wegner, W., Müller-Tidow, C., Horstmann, M., and Jücker, M. (2012). Leukemia-associated mutations in SHIP1 inhibit its enzymatic activity, interaction with the GM-CSF receptor and Grb2, and its ability to inactivate PI3K/AKT signaling. *Cell. Signal.* **24**, 2095–2101.
4. Kandell, W.M., Donatelli, S.S., Trinh, T.L., Calescibetta, A.R., So, T., Tu, N., Gilvary, D.L., Chen, X., Cheng, P., Adams, W.A., et al. (2020). MicroRNA-155 governs SHIP-1 expression and localization in NK cells and regulates subsequent infiltration into murine AT3 mammary carcinoma. *PLoS One* **15**, e0225820.
5. Miller, T.W., Rexer, B.N., Garrett, J.T., and Arteaga, C.L. (2011). Mutations in the phosphatidylinositol 3-kinase pathway: role in tumor progression and therapeutic implications in breast cancer. *Breast Cancer Res.* **13**, 224.
6. Ishihara, H., Sasaoka, T., Hori, H., Wada, T., Hirai, H., Haruta, T., Langlois, W.J., and Kobayashi, M. (1999). Molecular cloning of rat SH2-containing inositol phosphatase 2 (SHIP2) and its role in the regulation of insulin signaling. *Biochem. Biophys. Res. Commun.* **260**, 265–272.
7. Marcano, A.C.B., Burke, B., Gungadoo, J., Wallace, C., Kaisaki, P.J., Woon, P.Y., Farrall, M., Clayton, D., Brown, M., Dominiczak, A., et al. (2007). Genetic association analysis of inositol polyphosphate phosphatase-like 1 (INPPL1, SHIP2) variants with essential hypertension. *J. Med. Genet.* **44**, 603–605.
8. Paraiso, K.H.T., Ghansah, T., Costello, A., Engelman, R.W., and Kerr, W.G. (2007). Induced SHIP deficiency expands myeloid regulatory cells and abrogates graft-versus-host disease. *J. Immunol.* **178**, 2893–2900.

9. Kunkle, B.W., Grenier-Boley, B., Sims, R., Bis, J.C., Damotte, V., Naj, A.C., Boland, A., Vronskaya, M., van der Lee, S.J., Amlie-Wolf, A., et al. (2019). Genetic meta-analysis of diagnosed Alzheimer's disease identifies new risk loci and implicates Abeta, tau, immunity and lipid processing. *Nat. Genet.* **51**, 414–430.
10. Lambert, J.C., Ibrahim-Verbaas, C.A., Harold, D., Naj, A.C., Sims, R., Bellenguez, C., DeStafano, A.L., Bis, J.C., Beecham, G.W., Grenier-Boley, B., et al. (2013). Meta-analysis of 74,046 individuals identifies 11 new susceptibility loci for Alzheimer's disease. *Nat. Genet.* **45**, 1452–1458.
11. Jing, H., Zhu, J.X., Wang, H.F., Zhang, W., Zheng, Z.J., Kong, L.L., Tan, C.C., Wang, Z.X., Tan, L., and Tan, L. (2016). INPP5D rs35349669 polymorphism with late-onset Alzheimer's disease: A replication study and meta-analysis. *Oncotarget* **7**, 69225–69230.
12. Zajac, D.J., Simpson, J., Zhang, E., Parikh, I., and Estus, S. (2023). Expression of INPP5D Isoforms in Human Brain: Impact of Alzheimer's Disease Neuropathology and Genetics. *Genes* **14**, 763.
13. Gratuze, M., Leyns, C.E.G., and Holtzman, D.M. (2018). New insights into the role of TREM2 in Alzheimer's disease. *Mol. Neurodegener.* **13**, 66.
14. Peng, Q., Malhotra, S., Torchia, J.A., Kerr, W.G., Coggeshall, K.M., and Humphrey, M.B. (2010). TREM2- and DAP12-dependent activation of PI3K requires DAP10 and is inhibited by SHIP1. *Sci. Signal.* **3**, ra38.
15. Rosenthal, S.L., and Kamboh, M.I. (2014). Late-Onset Alzheimer's Disease Genes and the Potentially Implicated Pathways. *Curr. Genet. Med. Rep.* **2**, 85–101.
16. Wilkins, H.M., Carl, S.M., Greenlief, A.C.S., Festoff, B.W., and Swerdlow, R.H. (2014). Bioenergetic dysfunction and inflammation in Alzheimer's disease: a possible connection. *Front. Aging Neurosci.* **6**, 311.
17. Zhou, Y., Ulland, T.K., and Colonna, M. (2018). TREM2-Dependent Effects on Microglia in Alzheimer's Disease. *Front. Aging Neurosci.* **10**, 202.
18. Liu, Q., Shalaby, F., Jones, J., Bouchard, D., and Dumont, D.J. (1998). The SH2-containing inositol polyphosphate 5-phosphatase, ship, is expressed during hematopoiesis and spermatogenesis. *Blood* **91**, 2753–2759.
19. Pesesse, X., Deleu, S., De Smedt, F., Drayer, L., and Erneux, C. (1997). Identification of a second SH2-domain-containing protein closely related to the phosphatidylinositol polyphosphate 5-phosphatase SHIP. *Biochem. Biophys. Res. Commun.* **239**, 697–700.
20. Zhang, Y., Sloan, S.A., Clarke, L.E., Caneda, C., Plaza, C.A., Blumenthal, P.D., Vogel, H., Steinberg, G.K., Edwards, M.S.B., Li, G., et al. (2016). Purification and Characterization of Progenitor and Mature Human Astrocytes Reveals Transcriptional and Functional Differences with Mouse. *Neuron* **89**, 37–53.
21. Pedicone, C., Fernandes, S., Dungan, O.M., Dormann, S.M., Viernes, D.R., Adhikari, A.A., Choi, L.B., De Jong, E.P., Chisholm, J.D., and Kerr, W.G. (2020). Pan-SHIP1/2 inhibitors promote microglia effector functions essential for CNS homeostasis. *J. Cell Sci.* **133**, jcs238030.
22. An, H., Xu, H., Zhang, M., Zhou, J., Feng, T., Qian, C., Qi, R., and Cao, X. (2005). Src homology 2 domain-containing inositol-5-phosphatase 1 (SHIP1) negatively regulates TLR4-mediated LPS response primarily through a phosphatase activity- and PI-3K-independent mechanism. *Blood* **105**, 4685–4692.
23. Erneux, C., Edimo, W.E., Deneubourg, L., and Pirson, I. (2011). SHIP2 multiple functions: a balance between a negative control of PtdIns(3,4,5)P(3) level, a positive control of PtdIns(3,4)P(2) production, and intrinsic docking properties. *J. Cell. Biochem.* **112**, 2203–2209.
24. Stenton, G.R., Mackenzie, L.F., Tam, P., Cross, J.L., Harwig, C., Raymond, J., Toews, J., Wu, J., Ogden, N., MacRury, T., and Szabo, C. (2013). Characterization of AQX-1125, a small-molecule SHIP1 activator: Part 1. Effects on inflammatory cell activation and chemotaxis in vitro and pharmacokinetic characterization in vivo. *Br. J. Pharmacol.* **168**, 1506–1518.
25. Suwa, A., Yamamoto, T., Sawada, A., Minoura, K., Hosogai, N., Tahara, A., Kurama, T., Shimokawa, T., and Aramori, I. (2009). Discovery and functional characterization of a novel small molecule inhibitor of the intracellular phosphatase. *Br. J. Pharmacol.* **158**, 879–887.
26. Malbec, O., Fridman, W.H., and Daéron, M. (1999). Negative regulation of c-kit-mediated cell proliferation by Fc gamma RIIb. *J. Immunol.* **162**, 4424–4429.
27. Zhang, Y., Wavreille, A.S., Kunys, A.R., and Pei, D. (2009). The SH2 domains of inositol polyphosphate 5-phosphatases SHIP1 and SHIP2 have similar ligand specificity but different binding kinetics. *Biochemistry* **48**, 11075–11083.
28. Kato, K., Yazawa, T., Taki, K., Mori, K., Wang, S., Nishioka, T., Hamaguchi, T., Itoh, T., Takenawa, T., Kataoka, C., et al. (2012). The inositol 5-phosphatase SHIP2 is an effector of RhoA and is involved in cell polarity and migration. *Mol. Biol. Cell* **23**, 2593–2604.
29. Zhou, H., Yue, X., Wang, Z., Li, S., Zhu, J., Yang, Y., and Liu, M. (2021). Expression, purification and characterization of the RhoA-binding domain of human SHIP2 in E.coli. *Protein Expr. Purif.* **180**, 105821.
30. Ong, C.J., Ming-Lum, A., Nodwell, M., Ghanipour, A., Yang, L., Williams, D.E., Kim, J., Demirjian, L., Qasimi, P., Ruschmann, J., et al. (2007). Small-molecule agonists of SHIP1 inhibit the phosphoinositide 3-kinase pathway in hematopoietic cells. *Blood* **110**, 1942–1949.
31. Trésaugues, L., Silvander, C., Flodin, S., Welin, M., Nyman, T., Gräslund, S., Hammarström, M., Berglund, H., and Nordlund, P. (2014). Structural basis for phosphoinositide substrate recognition, catalysis, and membrane interactions in human inositol polyphosphate 5-phosphatases. *Structure* **22**, 744–755.
32. Paesmans, J., Martin, E., Deckers, B., Berghmans, M., Sethi, R., Loeys, Y., Pardon, E., Steyaert, J., Verstreken, P., Galicia, C., and Versées, W. (2020). A structure of substrate-bound Synaptojanin1 provides new insights in its mechanism and the effect of disease mutations. *Elife* **9**, e64922.
33. Le Coq, J., Camacho-Artacho, M., Velázquez, J.V., Santiveri, C.M., Gallego, L.H., Campos-Olivas, R., Dölker, N., and Lietha, D. (2017). Structural basis for interdomain communication in SHIP2 providing high phosphatase activity. *Elife* **6**, e26640.
34. Chamberlain, T.C., Cheung, S.T., Yoon, J.S.J., Ming-Lum, A., Gardill, B.R., Shakibakho, S., Dzanovic, E., Ban, F., Samiea, A., Jawanda, K., et al. (2020). Interleukin-10 and Small Molecule SHIP1 Allosteric Regulators Trigger Anti-inflammatory Effects through SHIP1/STAT3 Complexes. *iScience* **23**, 101433.
35. Le Coq, J., López Navajas, P., Rodrigo Martín, B., Alfonso, C., and Lietha, D. (2021). A new layer of phosphoinositide-mediated allosteric regulation uncovered for SHIP2. *Faseb. J.* **35**, e21815.
36. Krojer, T., Talon, R., Pearce, N., Collins, P., Douangamath, A., Brandao-Neto, J., Dias, A., Marsden, B., and von Delft, F. (2017). The XChemExplorer graphical workflow tool for routine or large-scale protein-ligand structure determination. *Acta Crystallogr. D Struct. Biol.* **73**, 267–278.
37. Pearce, N.M., Krojer, T., Bradley, A.R., Collins, P., Nowak, R.P., Talon, R., Marsden, B.D., Kelm, S., Shi, J., Deane, C.M., and von Delft, F. (2017). A multi-crystal method for extracting obscured crystallographic states from conventionally uninterpretable electron density. *Nat. Commun.* **8**, 15123.
38. McNicholas, S., Potterton, E., Wilson, K.S., and Noble, M.E.M. (2011). Presenting your structures: the CCP4mg molecular-graphics software. *Acta Crystallogr. D Biol. Crystallogr.* **67**, 386–394.
39. Mol, C.D., Izumi, T., Mitra, S., and Tainer, J.A. (2000). DNA-bound structures and mutants reveal abasic DNA binding by APE1 and DNA repair co-ordination [corrected]. *Nature* **403**, 451–456.
40. Beernink, P.T., Segelke, B.W., Hadi, M.Z., Erzberger, J.P., Wilson, D.M., 3rd, and Rupp, B. (2001). Two divalent metal ions in the active site of a new crystal form of human apurinic/aprimidinic endonuclease, Ape1: implications for the catalytic mechanism. *J. Mol. Biol.* **307**, 1023–1034.
41. Miroshnikova, A.D., Kuznetsova, A.A., Vorobjev, Y.N., Kuznetsov, N.A., and Fedorova, O.S. (2016). Effects of mono- and divalent metal ions on DNA binding and catalysis of human apurinic/aprimidinic endonuclease 1. *Mol. Biosyst.* **12**, 1527–1539.

42. Gucwa, M., Lenkiewicz, J., Zheng, H., Cymborowski, M., Cooper, D.R., Murzyn, K., and Minor, W. (2023). CMM-An enhanced platform for interactive validation of metal binding sites. *Protein Sci.* 32, e4525.
43. Infield, D.T., Rasouli, A., Galles, G.D., Chipot, C., Tajkhorshid, E., and Ahern, C.A. (2021). Cation- π Interactions and their Functional Roles in Membrane Proteins. *J. Mol. Biol.* 433, 167035.
44. Nelson, N., Wundenberg, T., Lin, H., Rehbach, C., Horn, S., Windhorst, S., and Jücker, M. (2020). Characterization of the substrate specificity of the inositol 5-phosphatase SHIP1. *Biochem. Biophys. Res. Commun.* 524, 366–370.
45. Chi, Y., Zhou, B., Wang, W.Q., Chung, S.K., Kwon, Y.U., Ahn, Y.H., Chang, Y.T., Tsujishita, Y., Hurley, J.H., and Zhang, Z.Y. (2004). Comparative mechanistic and substrate specificity study of inositol polyphosphate 5-phosphatase *Schizosaccharomyces pombe* Synaptojanin and SHIP2. *J. Biol. Chem.* 279, 44987–44995.
46. Waddell, G.L., Drew, E.E., Rupp, H.P., and Hansen, S.D. (2023). Mechanisms controlling membrane recruitment and activation of the auto-inhibited SHIP1 inositol 5-phosphatase. *J. Biol. Chem.* 299, 105022.
47. Pedicone, C., Fernandes, S., Matera, A., Meyer, S.T., Loh, S., Ha, J.H., Bernard, D., Chisholm, J.D., Paolicelli, R.C., and Kerr, W.G. (2022). Discovery of a novel SHIP1 agonist that promotes degradation of lipid-laden phagocytic cargo by microglia. *iScience* 25, 104170.
48. Winter, G., Waterman, D.G., Parkhurst, J.M., Brewster, A.S., Gildea, R.J., Gerstel, M., Fuentes-Montero, L., Vollmar, M., Michels-Clark, T., Young, I.D., et al. (2018). DIALS: implementation and evaluation of a new integration package. *Acta Crystallogr. D Struct. Biol.* 74, 85–97.
49. Evans, P.R., and Murshudov, G.N. (2013). How good are my data and what is the resolution? *Acta Crystallogr. D Biol. Crystallogr.* 69, 1204–1214.
50. Vonrhein, C., Tickle, I.J., Flensburg, C., Keller, P., Paciorek, W., Sharff, A., and Bricogne, G. (2018). Advances in automated data analysis and processing within autoPROC, combined with improved characterisation, mitigation and visualisation of the anisotropy of diffraction limits using STARANISO. *Acta Crystallogr. A Found. Adv.* 74, a360.
51. McCoy, A.J., Grosse-Kunstleve, R.W., Adams, P.D., Winn, M.D., Storoni, L.C., and Read, R.J. (2007). Phaser crystallographic software. *J. Appl. Crystallogr.* 40, 658–674.
52. Waterhouse, A., Bertoni, M., Bienert, S., Studer, G., Tauriello, G., Gumienny, R., Heer, F.T., de Beer, T.A.P., Rempfer, C., Bordoli, L., et al. (2018). SWISS-MODEL: homology modelling of protein structures and complexes. *Nucleic Acids Res.* 46, W296–W303.
53. Emsley, P., Lohkamp, B., Scott, W.G., and Cowtan, K. (2010). Features and development of Coot. *Acta Crystallogr. D Biol. Crystallogr.* 66, 486–501.
54. Murshudov, G.N., Skubák, P., Lebedev, A.A., Pannu, N.S., Steiner, R.A., Nicholls, R.A., Winn, M.D., Long, F., and Vagin, A.A. (2011). REFMAC5 for the refinement of macromolecular crystal structures. *Acta Crystallogr. D Biol. Crystallogr.* 67, 355–367.
55. Williams, C.J., Headd, J.J., Moriarty, N.W., Prisant, M.G., Videau, L.L., Deis, L.N., Verma, V., Keedy, D.A., Hintze, B.J., Chen, V.B., et al. (2018). MolProbity: More and better reference data for improved all-atom structure validation. *Protein Sci.* 27, 293–315.
56. Abraham, M.J., Murtola, T., Schulz, R., Páll, S., Smith, J.C., Hess, B., and Lindahl, E. (2015). GROMACS: High performance molecular simulations through multi-level parallelism from laptops to supercomputers. *SoftwareX* 1–2, 19–25.
57. Berendsen, H.J.C., van der Spoel, D., and van Drunen, R. (1995). GROMACS: A message-passing parallel molecular dynamics implementation. *Comput. Phys. Commun.* 91, 43–56.
58. Lindorff-Larsen, K., Piana, S., Palmo, K., Maragakis, P., Klepeis, J.L., Dror, R.O., and Shaw, D.E. (2010). Improved side-chain torsion potentials for the Amber ff99SB protein force field. *Proteins* 78, 1950–1958.
59. Fiser, A., Do, R.K., and Sali, A. (2000). Modeling of loops in protein structures. *Protein Sci.* 9, 1753–1773.
60. Lemkul, J. (2019). From Proteins to Perturbed Hamiltonians: A Suite of Tutorials for the GROMACS-2018 Molecular Simulation Package [Article v1.0]. *Living J. Comput. Mol. Sci.* 1.
61. Cox, O.B., Krojer, T., Collins, P., Monteiro, O., Talon, R., Bradley, A., Fedorov, O., Amin, J., Marsden, B.D., Spencer, J., et al. (2016). A poised fragment library enables rapid synthetic expansion yielding the first reported inhibitors of PHIP(2), an atypical bromodomain. *Chem. Sci.* 7, 2322–2330.
62. Collins, P.M., Ng, J.T., Talon, R., Nekrosiute, K., Krojer, T., Douangamath, A., Brandao-Neto, J., Wright, N., Pearce, N.M., and von Delft, F. (2017). Gentle, fast and effective crystal soaking by acoustic dispensing. *Acta Crystallogr. D Struct. Biol.* 73, 246–255.
63. Wright, N.D., Collins, P., Koekemoer, L., Krojer, T., Talon, R., Nelson, E., Ye, M., Nowak, R., Newman, J., Ng, J.T., et al. (2021). The Low-Cost, Semi-Automated Shifter Microscope Stage Transforms Speed and Robustness of Manual Protein Crystal Harvesting. *Acta Crystallogr. D Struct. Biol.* 77, 62–74.
64. Savitsky, P., Bray, J., Cooper, C.D.O., Marsden, B.D., Mahajan, P., Burgess-Brown, N.A., and Gileadi, O. (2010). High-throughput production of human proteins for crystallization: the SGC experience. *J. Struct. Biol.* 172, 3–13.

STAR★METHODS

KEY RESOURCES TABLE

REAGENT or RESOURCE	SOURCE	IDENTIFIER
Bacterial and virus strains		
BL21(DE3)-R3-pRARE2	Savitsky et al. ⁶⁴	RRID: Addgene_26242
DH10Bac	ThermoFisher	Cat#10361012
Sf9	ThermoFisher	Cat#11496015
Chemicals, peptides, and recombinant proteins		
cOmplete™ EDTA-free protease inhibitor cocktail	Sigma Aldrich	Cat#5056489001
Morpheus HT-96	Molecular Dimensions	Cat#MD1-46
Phosphate Sensor	ThermoFisher	Cat#PV4407
DSI-poised library	Enamine	Cat#DSI-860
Deposited data		
Apo structure	This study	PDB: 6IBD
Mg and PO ₄ bound structure	This study	PDB: 6XY7
Z2738285202 bound structure	This study	PDB: 8PDG
Z1742148362 bound structure	This study	PDB: 8PDH
Z1763271112 bound structure	This study	PDB: 8PDI
Z56948267 bound structure	This study	PDB: 8PDJ
Z2737076969 bound structure	This study	PDB: 5RW2
Z2064898339 bound structure	This study	PDB: 5RW3
Z19735192 bound structure	This study	PDB: 5RW4
Z69092635 bound structure	This study	PDB: 5RW5
Z2856434816 bound structure	This study	PDB: 5RW6
Z86622311 bound structure	This study	PDB: 5RW7
Z28290384 bound structure	This study	PDB: 5RW8
Z203581214 bound structure	This study	PDB: 5RW9
Z2856434812 bound structure	This study	PDB: 5RWA
Z2856434899 bound structure	This study	PDB: 5RWB
Z2856434879 bound structure	This study	PDB: 5RWC
Z1675346324 bound structure	This study	PDB: 5RWD
Z2856434865 bound structure	This study	PDB: 5RWE
Z1983897532 bound structure	This study	PDB: 5RWF
Z17497990 bound structure	This study	PDB: 5RWG
Z1152242726 bound structure	This study	PDB: 5RWH
Z2856434926 bound structure	This study	PDB: 5RWI
Z2856434824 bound structure	This study	PDB: 5RWJ
Z1267881672 bound structure	This study	PDB: 5RWK
Z1348371854 bound structure	This study	PDB: 5RWL
Z136583524 bound structure	This study	PDB: 5RWM
Z1310876699 bound structure	This study	PDB: 5RWN
Z2856434898 bound structure	This study	PDB: 5RWO
Z915492990 bound structure	This study	PDB: 5RWP
Z44592329 bound structure	This study	PDB: 5RWQ
Z2856434783 bound structure	This study	PDB: 5RWR
Z1478435544 bound structure	This study	PDB: 5RWS
Z32327641 bound structure	This study	PDB: 5RWT
Z57778470 bound structure	This study	PDB: 5RWU

(Continued on next page)

Continued

REAGENT or RESOURCE	SOURCE	IDENTIFIER
Z1103351268 bound structure	This study	PDB: 5RWV
Z2241115980 bound structure	This study	PDB: 5RWW
Z44567722 bound structure	This study	PDB: 5RWX
Z1259335913 bound structure	This study	PDB: 5RWY
Z57299529 bound structure	This study	PDB: 5RWZ
Z57258487 bound structure	This study	PDB: 5RX0
Z2466069494 bound structure	This study	PDB: 5RX1
Z1827898537 bound structure	This study	PDB: 5RX2
Z1262327505 bound structure	This study	PDB: 5RX3
Z1593306637 bound structure	This study	PDB: 5RX4
Z2443429438 bound structure	This study	PDB: 5RX5
Z30620520 bound structure	This study	PDB: 5RX6
Z1545196403 bound structure	This study	PDB: 5RX7
Z2856434884 bound structure	This study	PDB: 5RX8
Z54226095 bound structure	This study	PDB: 5RX9
Z54226095 bound structure	This study	PDB: 5RX9
Z2856434821 bound structure	This study	PDB: 5RXB
Z2856434868 bound structure	This study	PDB: 5RXC
Z111810692 bound structure	This study	PDB: 5RXD
Z240654968 bound structure	This study	PDB: 5RXE
Z2074076908 bound structure	This study	PDB: 5RXF
Z2856434909 bound structure	This study	PDB: 5RXG
Z939944666 bound structure	This study	PDB: 5RXH
Z2447286438 bound structure	This study	PDB: 5RXI
Z1722836661 bound structure	This study	PDB: 5RXJ
Z2856434840 bound structure	This study	PDB: 5RXK
Z1673618163 bound structure	This study	PDB: 5RXL
Z2856434894 bound structure	This study	PDB: 5RXM
Z68299550 bound structure	This study	PDB: 5RXO
Z2856434944 bound structure	This study	PDB: 5RXP
Z26548083 bound structure	This study	PDB: 5RXQ
Z1148747945 bound structure	This study	PDB: 5RXR
Z1818332938 bound structure	This study	PDB: 5RXS
Z319545618 bound structure	This study	PDB: 5RXT
Z2856434858 bound structure	This study	PDB: 5RXU
Z45527714 bound structure	This study	PDB: 5RXV
Z2856434856 bound structure	This study	PDB: 5RXW
Z1275599911 bound structure	This study	PDB: 5RXX
Z32014663 bound structure	This study	PDB: 5RXY
Z19739650 bound structure	This study	PDB: 5RXZ
Z275165822 bound structure	This study	PDB: 5RY0
Z2940170964 bound structure	This study	PDB: 5RY1
Z19727416 bound structure	This study	PDB: 5RY2
Z2027158783 bound structure	This study	PDB: 5RY3
Z300245038 bound structure	This study	PDB: 5RY4
Z166605480 bound structure	This study	PDB: 5RY5
Z198194394 bound structure	This study	PDB: 5RY6
Z1267773591 bound structure	This study	PDB: 5RY7
Z1374778753 bound structure	This study	PDB: 5RY8
Z274575916 bound structure	This study	PDB: 5RY9

(Continued on next page)

Continued

REAGENT or RESOURCE	SOURCE	IDENTIFIER
Z1741973467 bound structure	This study	PDB: 5RYA
Z927400026 bound structure	This study	PDB: 5RYB
Z18197050 bound structure	This study	PDB: 5RYC
Z955369596 bound structure	This study	PDB: 5RYD
Z33545544 bound structure	This study	PDB: 5RYE
Z1266823232 bound structure	This study	PDB: 5RYF
Z168883358 bound structure	This study	PDB: 5RYG
Z1212984951 bound structure	This study	PDB: 5RYH
Z274555794 bound structure	This study	PDB: 5RYI
Z2177153697 bound structure	This study	PDB: 5RYJ
Z1346370629 bound structure	This study	PDB: 5RYK
Z1745658474 bound structure	This study	PDB: 5RYL
HDX-MS data	This study	https://doi.org/10.5287/ora-py75jq8e5
Recombinant DNA		
INPP5DA-c132 (Ptase-C2: 6IBD)	This study	N/A
INPP5DA-c232 (Ptase-C2, all other work)	This study	N/A
INPPL1A-c231 (Ptase-C2)	This study	N/A
INPPL1A-c082 (Ptase)	This study	N/A
pS97SplitRBP_SHIP1-ΔC2 (Ptase)	Pedicone et al. ⁴⁷	RRID: Addgene_183769
pGTVL2	CMD in house vector	N/A
pFB-HGT-LIC	CMD in house vector	N/A
Software and algorithms		
Dials	Winter et al. ⁴⁸	https://dials.diamond.ac.uk
Aimless	Evans et al. ⁴⁹	https://ccp4.ac.uk
Staraniso	Vonrhein et al. ⁵⁰	https://staraniso.globalphasing.org
Phaser	McCoy et al. ⁵¹	https://ccp4.ac.uk
Swiss-Model	Waterhouse et al. ⁵²	https://swissmodel.expasy.org
Coot	Emsley et al. ⁵³	https://www2.mrc-lmb.cam.ac.uk/personal/pemsley/coot
Refmac5	Murshudov et al. ⁵⁴	https://ccp4.ac.uk
Molprobity	Williams et al. ⁵⁵	http://molprobity.biochem.duke.edu
Check My Metal	Gucwa et al. ⁴²	https://cmm.minorlab.org
Gromacs	Abraham et al. ⁵⁶ Berendsen et al. ⁵⁷	https://www.gromacs.org
Modloop	Fiser et al. ⁵⁹	https://modbase.compbio.ucsf.edu/modloop
XChem Explorer	Krojer et al. ³⁶	http://tkrojer.github.io/XChemExplorer
PanDDA	Pearce et al. ³⁷	https://pandda.bitbucket.io/pandda
Other		
IMAC Sepharose 6 Fast Flow	Cytiva	Cat#17092109
384 well microplate	Greiner	Cat#781906

RESOURCE AVAILABILITY

Lead contact

Further information and requests for resources and reagents should be directed to and will be fulfilled by the lead contact, William Bradshaw (william.bradshaw@cmd.ox.ac.uk)

Materials availability

All expression plasmids used in this study are available from the [lead contact](#) upon request. This study did not generate new, unique reagents.

Data and code availability

- Coordinates and structure factors for the reported structures have been deposited in the Protein DataBank (PDB) under accession codes given in the [key resources table](#) and are publicly available. MS data have been deposited with Oxford University Research Archive and are publicly available under the DOI given in the [key resources table](#).
- This paper does not report original code.
- Any additional information required to reanalyse the data reported in this paper is available from the [lead contact](#) upon request.

EXPERIMENTAL MODEL AND STUDY PARTICIPANT DETAILS

Protein used in this study was expressed in either Rosetta cells (BL21(DE3)-R3-pRARE2) grown in TB or Sf9 cells grown in Sf-900 II SFM the “[method details](#)” section gives more details.

METHOD DETAILS

Cloning

LIC primers were designed corresponding to residues Glu396 to Gln856 of human SHIP1 (SHIP1-Ptase-C2) and the pGTVL2 (used for 6IBD) and pFB-HGT-LIC vectors (used for all other work). The PCR product was ligated into the two vectors with the former transformed into Rosetta cells (BL21(DE3)-R3-pRARE2) and the latter into DH10Bac for use with the Bac-to-Bac system. SHIP2 constructs coding for Glu420 to Ser743 (SHIP2-Ptase) and Glu420 to Arg878 (SHIP2-Ptase-C2) were similarly cloned into pFB-HGT-LIC. Successful DH10Bac transformants were identified through blue/white screening and the bacmid was purified from 2 mL overnight cultures supplemented with appropriate antibiotics. The SHIP1 construct coding for Asn392 to Gln729 in pS97splitRBP (SHIP1-Ptase, SHIP1ΔC2) was received from William Kerr and Sandra Fernandes and transformed into Rosetta cells.⁴⁷

Protein expression

Bacterial expression

One 50 mL and two 10 mL overnight LB cultures inoculated from glycerol stocks were grown in a 250 mL conical flask and 50 mL falcon tubes respectively, each with 50 μg/mL kanamycin and 34 μg/mL chloramphenicol at 37°C with shaking at 250 rpm. The following morning, the cultures were combined and 10 mL was used to inoculate each of six 1L TB cultures with 50 μg/mL kanamycin. They were grown at 37°C with shaking at 180 rpm. Once the cultures had reached an OD₆₀₀ between 1.5 and 2.0, the temperature was reduced to 18°C and, 30 min later, expression was induced by addition of 300 μM IPTG. Cultures were grown overnight and harvested by centrifugation at 6,000g the following morning. Pellets were scraped into falcon tubes and flash frozen in liquid nitrogen.

Insect cell expression

It was observed that some SHIP1 and SHIP2 constructs produce a significantly greater yield through insect cell expression. The constructs were expressed in Sf9 cells grown in Sf-900 II SFM. Each liter of cells at a density of 0.2×10^6 /mL was infected with 3 mL of P2 viruses and allowed to grow for approximately 68 h at 27°C. Cells were harvested by centrifugation at 1500g, flash frozen in liquid nitrogen and stored at −80°C.

Protein purification

For bacterially expressed protein, 6 L of expression pellets were thawed by immersing the tubes in water and were resuspended in lysis buffer (50 mM HEPES pH 7.5, 500 mM NaCl, 20 mM imidazole, 5% glycerol, 1 mM TCEP) to a total volume of 240 mL per 3 L of expression pellet. For protein expressed in Sf9 cells, 2L Expression pellets handled in the same way were resuspended in lysis buffer to 240 mL supplemented with EDTA-free protease inhibitors. The cells were lysed by sonication on ice with 5 s on, 10 s off for a total of 20 min for *E. coli* and 15 min for Sf9. The lysate was mixed halfway through sonication. Once lysis was complete, the lysate was cleared by centrifugation at 75,000g for 20 min.

After prewashing 3 mL of nickel beads in lysis buffer, they were added to the supernatant and split into several 50 mL falcon tubes. The tubes were then rotated in a cold room for 1 h. Subsequently, the beads were pelleted by centrifugation at 800g for 5 min and washed twice with lysis buffer before being pelleted again.

The beads were resuspended in 20 mL lysis buffer and loaded on to a gravity column. The resin was washed with 10 mL wash buffer (50 mM HEPES pH 7.5, 500 mM NaCl, 40 mM imidazole, 5% glycerol, 1 mM TCEP) before the protein was eluted with three 10 mL washes with elution buffer (50 mM HEPES pH 7.5, 500 mM NaCl, 300 mM imidazole, 5% glycerol, 1 mM TCEP).

TEV protease was added to the eluate at a concentration (mg/mL) of 5:1 target protein:TEV. The mixture was dialyzed overnight into dialysis buffer (50 mM HEPES pH 7.5, 500 mM NaCl, 5% glycerol, 1 mM TCEP) at 4°C. The TEV protease was removed by passing the sample back down the nickel column, equilibrated with lysis buffer, followed by a wash with 10 mL lysis buffer. The flow through and wash fractions were combined and concentrated to a volume of 1 mL. This was passed down a Superdex 200 16/60 column in gel filtration buffer (50 mM HEPES pH 7.5, 250 mM NaCl, 5% glycerol, 1 mM TCEP). Selected fractions were combined and concentrated to around 6 mg/mL.

Structure determination

Crystallisation

Crystallisation conditions for SHIP1-Ptase-C2 were screened at 20°C by sitting drop vapor diffusion using 150 nL drops with ratios of 2:1, 1:1 and 1:2. Screens were set up around identified conditions and the best crystals took around 1 to 2 weeks to grow in 0.1M bis-tris pH 7.0, 14% PEG2KMME, 12% PEG3350. The crystals were cryoprotected by addition of 1 μ L reservoir to the drop. The apo structure was determined from crystals grown in these conditions. These crystals were also used for seeding. Crystals from 6 drops were resuspended in a total of 30 μ L reservoir solution with a seed bead. The seed stock was vortexed for 10 s three times with 30 s on ice between each. This was then diluted 100-fold in reservoir solution and conditions were rescreened with 20 nL seeds added to 150 nL drops. Crystals were observed in Molecular Dimensions Morpheus C1 (30 mM sodium phosphate, ammonium sulfate, sodium nitrate, 100 mM MES/imidazole pH 6.5, 10% PEG 20,000, 20% PEG 500 MME) after around a week. For the magnesium and phosphate bound structure, these crystals were cryoprotected by addition to the drop of 1 μ L reservoir solution supplemented with 2mM MgCl₂.

Data collection and processing

Data were collected at Diamond Light Source beamline I03. Apo data were integrated using Dials⁴⁸ and scaled with Aimless⁴⁹ to a resolution of 1.48 Å, while the data for the magnesium and phosphate bound structure were scaled with Staraniso⁵⁰ and Aimless. An elliptical high-resolution cut-off of between 1.34 Å and 1.09 Å was applied. Molecular replacement was performed using Phaser⁵¹ with a model generated by Swiss-Model⁵² based on chain B of the structure of SHIP2 (5OKM) and refined with successive rounds of Coot⁵³ and Refmac5.⁵⁴ The apo structure was refined to an R_{work} of 0.174 and an R_{free} of 0.200 while the magnesium and phosphate bound structure was refined to an R_{work} of 0.136 and an R_{free} of 0.157. The final models were verified with MolProbity.⁵⁵ The magnesium ion was verified with Check My Metal⁴² and the structures were deposited in the PDB under accession codes 6IBD and 6XY7.

Activity assays

The phosphatase activity of SHIP1 and SHIP2 was determined by measuring inorganic phosphate production using Phosphate Sensor. Soluble inositol 1,3,4,5-tetraphosphate (I(1,3,4,5)P₄) and phosphatidylinositol 3,4,5-trisphosphate-DiC8 (PI(3,4,5)P₃-DiC8) were used as substrates. Briefly, 10 μ L enzyme (SHIP1 Ptase (50 nM), SHIP1 Ptase-C2 (50 nM), SHIP2 Ptase (50 nM) or SHIP2 Ptase-C2 (15 nM) (final assay concentration)) in assay buffer (20 mM HEPES pH 7.5, 5 mM MgCl₂, 150 mM NaCl, 0.01% Triton X-100 and 0.1% BSA) was added to clear-bottomed black 384-well plates. Phosphate Sensor, 20 μ L at 1.5 μ M (final concentration of 0.75 μ M), was added and the plate centrifuged at 1000 rpm for 1 min and left to incubate at RT for 30 min. Substrates, 10 μ L at 4X the final assay concentration, were added to start the reaction via the internal liquid handling function of the FLIPR Tetra (molecular devices) and the increase in fluorescence produced via phosphate binding to the Phosphate Sensor was monitored over time (λ_{ex} = 390–420 nm and λ_{em} = 475–535 nm). Measurements were performed in triplicate. A dose response of the substrate was performed with a top final assay concentration of 100 μ M. A phosphate standard curve was used to interpolate the concentration of phosphate produced from raw RFU values. Progress curves were normalised to the substrate alone at each concentration to account for phosphate contamination of the substrate and the initial rate of phosphate production was plotted vs. substrate concentration and fitted to the Michaelis-Menten equation to obtain K_m and k_{cat} . All data analysis was carried out in GraphPad Prism.

Hydrogen-deuterium exchange

HDX-MS experiments were performed using a Synapt G2Si HDMS coupled to an Acquity UPLC system with HDX-MS and automation (Waters Corporation, UK).

Labeling was performed using a continuous labeling workflow at 20°C. Each protein was diluted to 10 μ M in equilibration buffer (PBS, pH 7.4). Labeling was initiated by diluting 5 μ L of each protein to 50 μ L total volume by addition of labeling buffer (PBS prepared in D₂O, pD 7.4) giving a 90% D₂O environment. Labeling took place for various time points. The labeling reaction was quenched by a 1:1 addition of ice-cold quench buffer (50 mM KH₂PO₄, 1 M GdmCl, pH 2). Proteins were digested online with a Waters Enzymate BEH pepsin column at 20°C. Peptides were trapped on a Waters BEH C18 VanGuard pre-column for 3 min at a flow rate of 200 μ L/min in buffer A (0.1% formic acid ~ pH 2.5) before being applied to a Waters BEH C-18 analytical column. Peptides were eluted with a linear gradient of buffer B (0.1% formic acid in acetonitrile ~ pH 2.5) at a flow rate of 40 μ L/min. All trapping and separation were performed at ~0°C to reduce back exchange.

MS data were acquired using MSE workflow. All time points across this experiment were obtained in triplicate. MS was calibrated separately using Nal and the MS data were obtained with lock mass correction using LeuEnk. Peptides were assigned with the ProteinLynx Global Server (PLGS, Waters Corporation, UK) software and the isotope uptake of respective peptides was determined using DynamX v3.0.

Molecular dynamics

Simulations were performed using Gromacs 2018.3^{56,57} with the AMBER99SB*-ILDN force field.⁵⁸ SHIP1 L4-in simulations used the apo structure presented here, SHIP2 L4-out simulations used chain B of 5OKM, SHIP2 L4-in simulations used the phosphatase domain of 3NR8 joined to the C2 domain from 5OKM chain B. Each of these simulations was performed with and without the C2 domain. The linker between the phosphatase and C2 domains was modeled with ModLoop.⁵⁹ Simulations used parameters based on those in the Gromacs lysozyme tutorial.⁶⁰ The structures were prepared for full MD runs by energy minimisation followed by 100 ps

temperature, pressure and density equilibration steps. MD runs were initially performed for 1 μ s. As the SHIP2 L4-in simulations showed hydrogen bonds forming after approximately 950 ns (Figure 5D), these simulations were extended to 2 μ s.

Figures 5A, 5C and 5E were calculated from the average RMSFs across the three repeats of each simulation. Averaging distances across simulations does not make sense so the data used for Figures 5B, 5D and 5F are from a single representative simulation. Those for B were selected to most strongly agree with the conclusions reached by Le Coq et al.,³³ although the other two also agreed. The phosphatase domain data used in 5D are similar to the data from the other two repeats with hydrogen bonds able to form briefly. The hydrogen bonds only formed very briefly in the other Ptase-C2 simulations, but the data shown demonstrate this formation well. The data were similar for all six SHIP1 simulations.

Crystallography-based fragment screening

Fragment screening was performed using the XChem pipeline at Diamond Light Source. Several hundred crystals were produced using seeding and Morpheus C1, as described above without the addition of MgCl_2 . Several crystals grown in these conditions were screened to confirm that the diffraction was routinely of a high quality and to a high resolution. Initial screening of DMSO soaked crystals showed a deterioration in diffraction quality from around 20–25% DMSO. Fragments from the DSI-posed library⁶¹ were therefore soaked into crystals to a final DMSO concentration of 15% (a fragment concentration of 75 mM) using a Labcyte Echo⁶² and allowed to incubate for between 2 and 5 h. Crystals were fished from drops with the aid of a Shifter,⁶³ allowing approximately 200 crystals to be fished per hour. Data were collected automatically on beamline I04-1 using X-ray centring and a rapid data collection protocol (0.48° oscillations, 0.04 s exposures, 375 images). The resulting datasets were processed using XChem Explorer and PanDDA.^{36,37} Fragment bound structures can be viewed on Fragalysis (<http://fragalysis.diamond.ac.uk>) and have been deposited in the PDB using accession codes 5RW2 to 5RYL and group deposition G_1002180.

Mass spectrometry-based screen

Sample preparation

An in-house library of 1920 covalent small molecule fragments was dispensed in 10 nL aliquots between 7 × 384 well microplates. 12.5 μ L of SHIP1-Ptase-C2 in 50 mM HEPES pH 7.5, 250 mM NaCl, 5% glycerol and 1 mM TCEP was added to each well at a concentration of 85 μ g/mL to give a final ligand concentration of approximately 0.2 mM. The reaction was left overnight at room temperature and terminated by adding 50 μ L of 0.2% formic acid.

LC-MS screening

Reversed-phase HPLC was performed in-line prior to mass spectrometry. A 50 μ L aliquot with SHIP1-Ptase-C2 with covalent library compounds was injected on to a 2.1 mm × 12.5 mm Zorbax 5 μ M 300SB-C3 guard column housed in a column oven set at 40°C. The solvent system used consisted of solvent A: 0.1% formic acid and solvent B: 0.1% formic acid in methanol. Chromatography was performed as follows: initial conditions were 90% A and 10% B and a flow rate of 1.0 mL/min. After 15 s at 10% B, a linear gradient to 80% B was applied over 45 s and then to 95% B over 3 s. Elution then proceeded isocratically at 95% B for 1 min 12 s followed by equilibration at initial conditions for a further 45 s. Protein and covalent inhibitor denaturing intact mass was determined using an MSD-ToF electrospray ionisation orthogonal time-of-flight mass spectrometer (Agilent Technologies Inc. – Palo Alto, CA, USA). The instrument was configured with the standard ESI source and operated in positive ion mode. The ion source was operated with the capillary voltage at 4000 V, nebulizer pressure at 60 psi, drying gas at 350°C and drying gas flow rate at 24 L/min. The instrument ion optic voltages were as follows: fragmentor 250 V, skimmer 60 V and octopole RF 250 V. This LC-MS method was applied to each well of the 7 microplates in 384 well format. Data analysis was performed using Agilent MassHunter Qualitative Analysis.

Crystallographic soaks

The top 20 hits from the MS screen were selected and soaks were performed by adding the compounds in DMSO to Morpheus C1 to a final concentration of 5 mM, 20% DMSO. 1 μ L of this was added to drops containing crystals and incubated at 20°C for one day before harvesting. Data were collected and processed as previously stated.

QUANTIFICATION AND STATISTICAL ANALYSIS

Crystallographic and refinement statistics are reported in Table 1 and Data S1. Activity assay data are reported in Table 2. Methods and software used for analysis of crystallographic and data from activity assays, HDX-MS, and molecular dynamics are reported in respective sub-sections of the “method details” section. Tests of statistical significance were performed on HDX-MS data using the software listed in the relevant methods section.

Structure, Volume 32

Supplemental Information

Regulation of inositol 5-phosphatase

activity by the C2 domain of SHIP1 and SHIP2

William J. Bradshaw, Emma C. Kennedy, Tiago Moreira, Luke A. Smith, Rod Chalk, Vittorio L. Katis, Justin L.P. Benesch, Paul E. Brennan, Emma J. Murphy, and Opher Gileadi

Table S1 – The 20 best MS screen hits – Related to the mass spec screen

Enamine code	SMILES	Result of soak
Z2738285202	<chem>C1C=CC=C2C=CC(NC(=O)C=C)=NC12</chem>	Bound – 8PDG
Z44303404	<chem>COC=1C=CC(C=C(C#N)C(=O)O)=CC1</chem>	Not bound
Z2865977938	<chem>CCC=1OC=2C=CC=CC2C1C=C(C#N)C(=O)N</chem>	Not bound
Z2738282628	<chem>C=CC(=O)NC=1C=C2C=CC=CN2N1</chem>	Not bound
Z1688701829	<chem>FC(F)(F)C(=O)N1CCCC1C(=O)CCl</chem>	Not bound
Z1742148362	<chem>N#CC1=NN=C(O1)C=2C=CC=CC2</chem>	Bound – 8PDH
Z1763271112	<chem>N#CC1=NN=C(S1)C=2C=CC=CC2</chem>	Bound – 8PDI
Z56948267	<chem>FC=1C=C(SC#N)C=CC1NC(=O)CCl</chem>	Bound – 8PDJ
Z118281008	<chem>OC(=O)C(=CC=1C=NN(C1)C=2C=CC=CC2)C#N</chem>	Not bound
Z166653162	<chem>FS(=O)(=O)CCN1N=NC(=N1)C=2C=CC=CC2</chem>	Not bound
Z1263529582	<chem>Cl.O=C(NC1CCNCC1)OC=2C=CC=CC2</chem>	Not bound
Z2736967631	<chem>CC=1C=CC(NS(=O)(=O)CCCS(=O)(=O)F)=NC1</chem>	Not bound
Z1354075704	<chem>FS(=O)(=O)C#CC=1C=CC=CC1</chem>	Not bound
Z2734668359	<chem>FS(=O)(=O)CCSC1=NC=2C=CC=CC2O1</chem>	Not bound
Z1269155601	<chem>NS(=O)(=O)C=1C=CC=C(C1)S(=O)(=O)F</chem>	Not bound
Z2867526346	<chem>COC=1C=C(C=C(C#N)C(=O)NC(C)C)SN1</chem>	Not bound
Z2737463623	<chem>N#CC(=CC1=CSN=N1)C=2C=CC=CN2</chem>	Not bound
Z2867512903	<chem>CC1=CC(NS(=O)(=O)C2=CCCCC2)=CNC1=O</chem>	Not bound
Z3376082211	<chem>CC(C)(C)OC(=O)N1CC(C1)OCCS(=O)(=O)F</chem>	Not bound
Z1649581806	<chem>C1C=CC(=CC1)S(=O)(=O)C=CC#N</chem>	Not bound

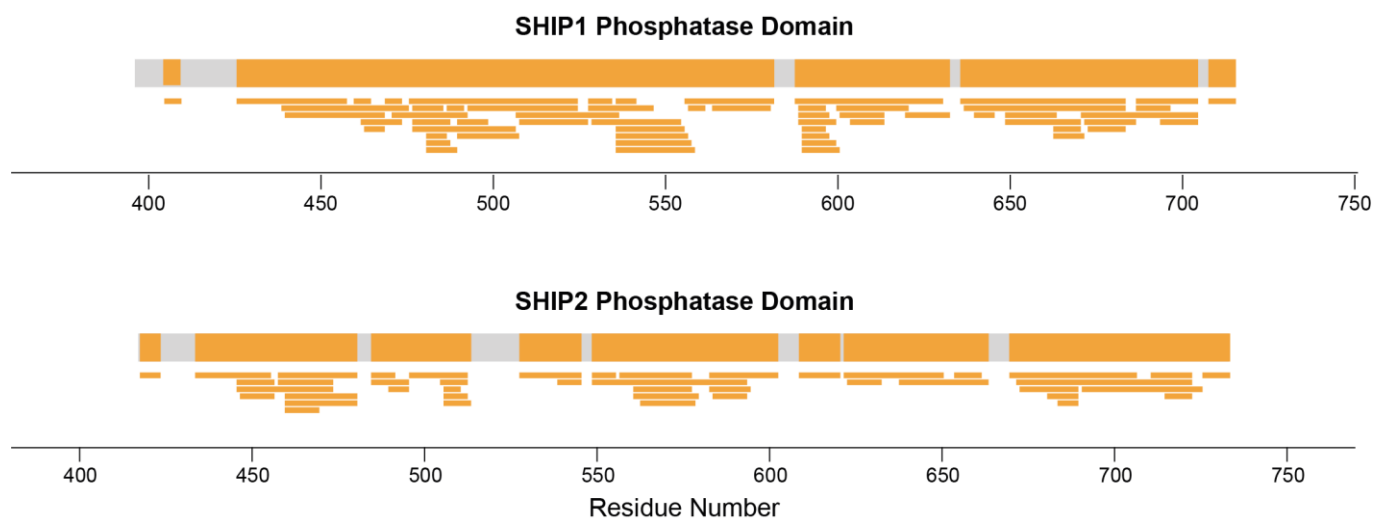


Figure S1 – HDX-MS coverage map – Related to figure 4. Regions of the phosphatase domains of SHIP1 and SHIP2 observed in HDX-MS are shown in orange with regions not observed shown in grey. Individual detected peptides are shown below.

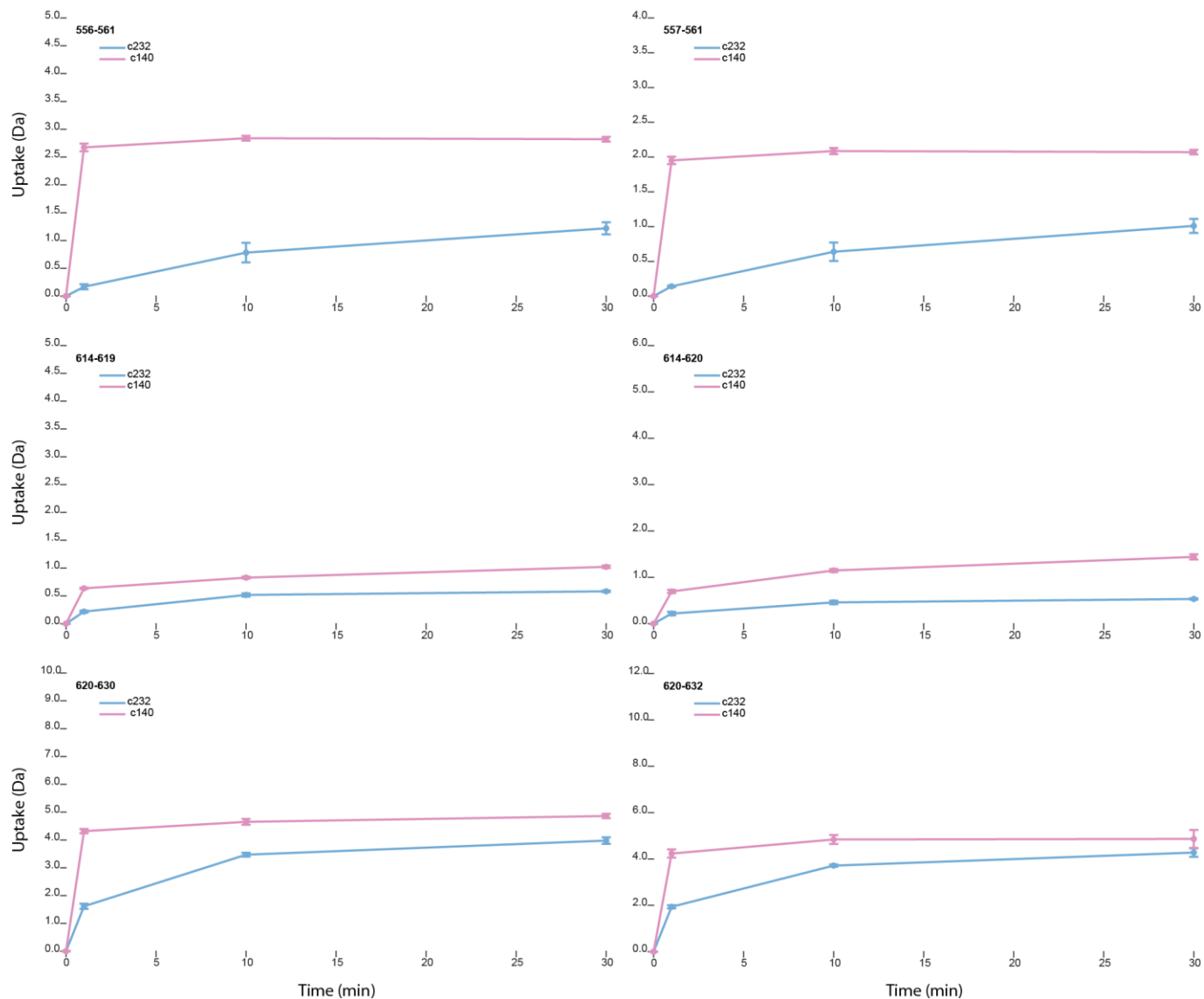


Figure S2 – SHIP1 uptake plots – Related to figure 4. Examples of peptides detected that showed significantly greater uptake in the construct without the C2 domain than with.

Figure S3

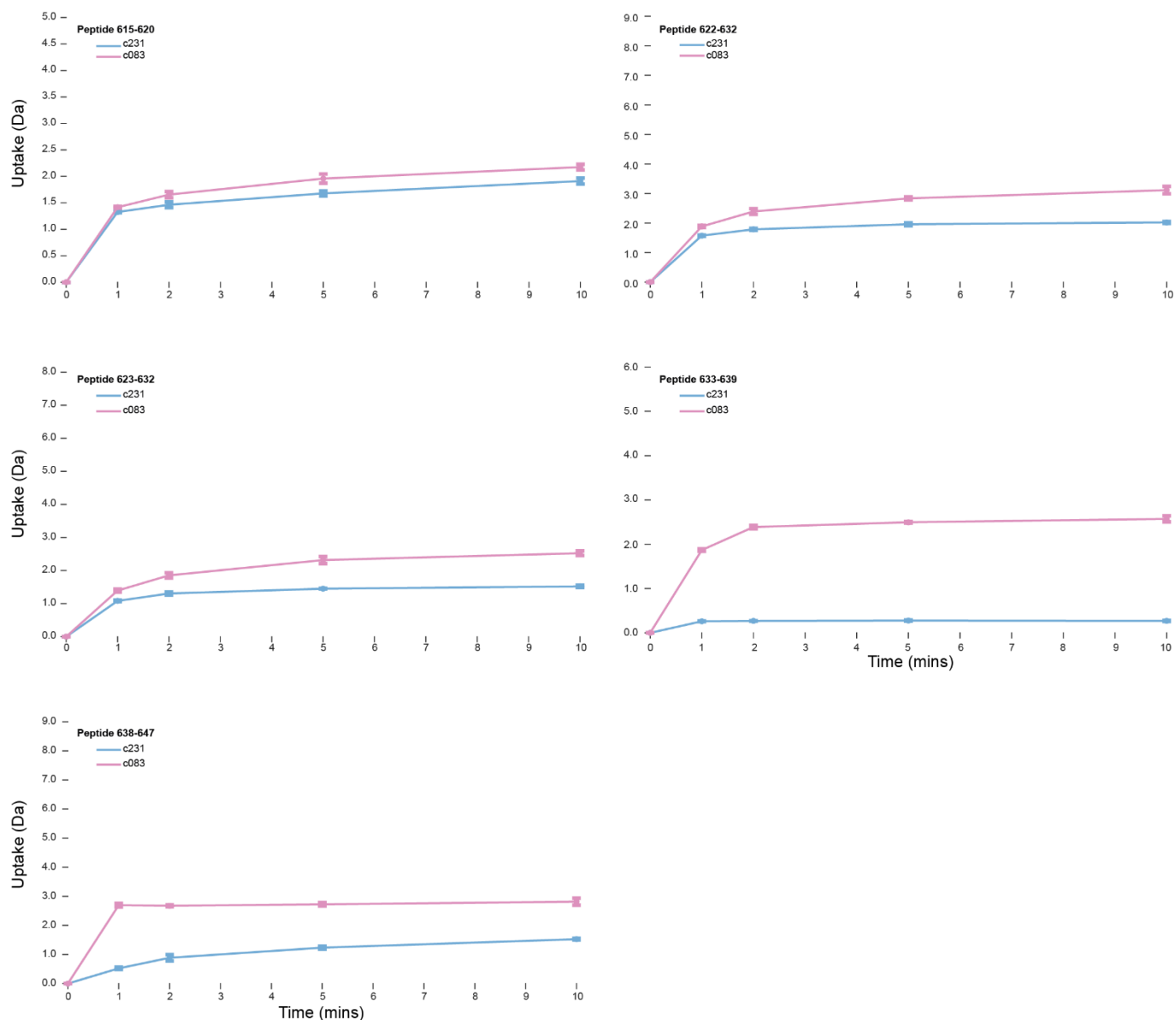


Figure S3 – SHIP2 uptake plots – Related to figure 4. Examples of peptides detected that showed significantly greater uptake in the construct without the C2 domain than with. All plots shown are for peptides in the region of helices 5, 6 and 7.